Universidade de Aveiro Departamento de Geociências
Ano 2013

ARSLAN SHAHBAZ

RECONSTRUÇÃO PALEOAMBIENTAL E ESTATIGRÁFICA DA BACIA DO SADO (PORTUGAL)

PALEOENVIRONMENTAL AND STRATIGRAPHIC RECONSTRUCTION OF SADO BASIN (PORTUGAL)

Universidade de Aveiro Departamento de Geociências
Ano 2013

ARSLAN SHAHBAZ

RECONSTRUÇÃO PALEOAMBIENTAL E ESTATIGRÁFICA DA BACIA DO SADO (PORTUGAL)

PALEOENVIRONMENTAL AND STRATIGRAPHIC RECONSTRUCTION OF SADO BASIN (PORTUGAL)

Dissertation submitted to the University of Aveiro to fulfill the requirements for the degree of Master of Engineering Geology, held under the scientific guidance of Dr. Fernando Joaquim Tavares Fernandes Rocha, Professor, Department of Geosciences, University of Aveiro.

Funded by the Erasmus Mundus International Master in advanced clay science (IMACS) scholarship.

I dedicate this work to all portuguese people for the love and support they provided me during my stay in Portugal.

o júri / the jury

presidente / president

Prof. Doutor Fernando Joaquim Tavares Rocha
professor catedrático da Universidade de Aveiro

vogais / examiners committee

Doutora Slavka Andrejkovicova
Investigadora do centro GEOBIOTEC; Departamento de Geociências da Universidade de Aveiro

Doutora Ana Carina Tavares Quintela dos Santos
Investigadora do centro GEOBIOTEC; Departamento de Geociências da Universidade de Aveiro

Acknowledgment

The completion of this work would not have been possible without the support of many people who helped me during the journey of my work.

I am thankful to Professor Fernando Rocha for his guidance and very unique style of scientific discussions which I always liked a lot.

I find no appropriate words in dictionary to thank Ana Carina for being always ready to help me and for her patience to address my all kind of questions. She always proved to be a life saving angel for me whenever I encountered any problem.

I am also very indebted to Cristiana Costa, Walid and Slavka for providing a nice environment in the lab. I would like to pass my gratitude to Joao, Denise, Cristina for providing me the lab results.

I am thankful to my colleagues and staff of the Department of Geoscience contributing to a good working environment and solving practical problems and bureaucratic issues.

A special thanks to my family whom I missed a lot but they always encouraged me.

This work was funded by the Erasmus Mundus International Master in advanced clay science (IMACS) scholarship.

keywords

Clay minerals, palygorskite, basin analysis, paleoenvironmental reconstruction, lithostratigraphical markers, diagenesis.

Abstract

The Tertiary deposits of the Sado Basin (in southwestern Portugal) were deposited in a typical continental basin, composed by 4 main lithostratigraphic units. During the Palaeogene, the Sado Basin was a closed basin in which the mineralogy of the primary facies underwent significant changes that resulted in the extensive occurrence of palygorskite. The Palaeogene fill of the Sado basin is composed by reddish coarse detrital sediments (conglomerates, arkosic sandstones, clays and marly carbonates). 28 samples representative of the most exposed outcrops of these units were collected and analysed by XRD, XRF and SEM-EDS for their mineralogical and chemical characterization. SEM-EDS was used to compute the crystallochemical formulas for the identified clay minerals. Clay minerals associations were used as lithostratigraphical markers as well as for paleoenvironmental reconstructions and diagenesis analyses. Palaeogene deposits are characterized by an increase on palygorskite relative amounts in the distal parts of the basin as well as by higher structural order of the clay minerals in the Miocene sediments and lower structural order in Eocene sediments, pointing to a significant diagenesis contribution.

palavras-chave Minerais argilosos, paligorskite, análise de bacias, reconstrução paleoambiental, marcadores litoestratigráficos, diagénese.

Resumo

Os depósitos terciários da Bacia do Sado (no sudoeste de Portugal) comtemplam quatro principais unidades litoestratigráficas que resultam de uma deposição típica de uma bacia continental. Durante o Paleogénico, a Bacia do Sado era uma bacia fechada em que a mineralogia da fácies primária passou por mudanças significativas, que resultou numa extensa ocorrência de paligorskite. O preenchimento paleogénico da bacia do Sado é composto por sedimentos avermelhados detríticos grosseiros (conglomerados, arcoses, argilas e margas). Foram colhidas 28 amostras representativas dos afloramentos mais expostos das referidas unidades litoestratigráficas e analisadas, do ponto de vista mineralógico e químico, por DRX, FRX, respectivamente. Recorreu-se a análises SEM-EDS para calcular as fórmulas cristaloquímicas para os minerais argilosos identificados. Os resultados obtidos permitiram estabelecer associações mineralógicas para cada unidade, principalmente no que concerne os minerais argilosos. Estas associações foram interpretadas como marcadores litostratigráficos e possibilitaram a reconstrução paleoambiental e análise diagenética da bacia do Sado. De forma geral, os depósitos paleogénicos que preenchem a Bacia do Sado são caracterizados por um incremento na quantidade relativa de paligorskite no sentido proximal-distal, bem como por um aumento da ordem estrutural dos minerais de argila na mesma unidade litoestratigráfica, o que aponta para uma contribuição diagenética relevante.

Table of Contents

Index of Figures

Index of Tables

Annex-Diffractograms of Samples

Fig.20- Diffractograms of sample S1, powder, natural, glycolated and at 500°C

Fig.21- Diffractograms of sample S2, powder, natural, glycolated and at 500°C

Fig.22- Diffractograms of sample S3, powder, natural, glycolated and at 500°C

Fig.23- Diffractograms of sample S4, powder, natural, glycolated and at 500°C

Fig.24- Diffractograms of sample S5, powder, natural, glycolated and at 500°C

Fig.25- Diffractograms of sample S6, powder, natural, glycolated and at 500°C

Fig.26- Diffractograms of sample S7, powder, natural, glycolated and at 500°C

Fig.27- Diffractograms of sample S8, powder, natural, glycolated and at 500°C

Fig.28- Diffractograms of sample S9, powder, natural, glycolated and at 500°C

Fig.29- Diffractograms of sample S10, powder, natural, glycolated and at 500°C

Fig.30- Diffractograms of sample S11, powder, natural, glycolated and at 500°C

Fig.31- Diffractograms of sample S12, powder, natural, glycolated and at 500°C

Fig.32- Diffractograms of sample S13, powder, natural, glycolated and at 500°C

Fig.33- Diffractograms of sample S14, powder, natural, glycolated and at 500°C

1. Introduction

Stratigraphic interpretation using clay-mineral analysis can be made when the diagenetic influence on clay mineralogy remains low. The spatio-temporal distribution of detrital clay minerals in sedimentary successions may provide information on the environmental conditions of the source areas such as climate lithology and soils composition (Adatte and Bolle, 2001; Alcalá et al., 2001; Ruffell et al., 2002; Dou et al., 2010), relative sea-level changes (Daoudi et al., 1995; Moon et al., 2000; Wang et al., 2006; Clark et al., 2009), and tectonics (Enu, 1986; Martín-Martín et al., 2001). This distribution can indicate the proximity to the source area (Thiry and Jacquin, 1993; Clark et al., 2009), with implications for palaeoenvironmental modeling. Stratigraphic changes in the abundance of smectite, kaolinite, and illite allow assessments of relative proximal–distal variations.

The analysis of the clay mineral associations' provides important information on paleoclimatic studies essentially concerning regional data. The composition of detrital mineral associations is particularly useful in the way that they record the modifications that occur in source area, in what concerns the erosion conditions (Rocha et al., 2005).

Palygorskite is relatively rare in nature; however, its origins has been studied frequently owing to the unique conditions required for its formation and stability, and the need to find new commercial deposits. According to Callen (1984), major deposits of palygorskite were formed in three different environments: (1) in epicontinental and inland seas and lakes as chemical sediments or by reconstitution of former sedimentary clays; (2) in the open ocean in association with fore-arc basins and ocean ridges by hydrothermal alteration of basaltic glass, volcaniclastic sediments or existing clays; and (3) in calcareous soils by direct crystallization. With respect to their geotectonic setting, neoformed palygorskite and sepiolite are predominant in shallow shelf basins on passive margins or intraplate basins. Continental rift basins, continental “sag” basins or some perimarine basins, tend to contain significant deposits of these minerals, commonly formed in saline or hypersaline conditions Merriman, 2005).

According to Singer (1984), palygorskite in soils is associated with one of the following conditions: (i) modern soils that, at present or in the past, were affected by rising groundwater of pH 7–8 and high salinity; (ii) in soils with distinct and sharp textural transitions because these minerals accumulate in the coarse fraction (this group includes many palaeosols); and (iii) in calcretes (caliches). In all these cases, palygorskite (and very rarely sepiolite, when Al is absent or immobilized) is precipitated by evaporation of the vadose water (Jones and Weir, 1983). Soils (duricrusts) can be cemented by palygorskite named palycretes (Rodas et al., 1994).

The present research project was executed under the title, “Paleoenvironmental and stratigraphic reconstruction of Sado Basin (Portugal)”. This research work was carried out for the fulfillment of International Master in Advanced Clay Science (IMACS) degree. This thesis is the outcome of findings of fieldwork and laboratory investigations to decipher the paleoenvironmental model and marking of stratigraphic boundaries in the tertiary sedimentary sequence of the Sado basin, Portugal, using clay minerals assemblage as a valuable tool. This work has been divided into two parts. First part is focused on the the marking of stratigraphic boundaries between different sedimentary units and second part is concerned about the reconstruction of paleoenvironmental model and mechanism of genesis of palygorskite in Sado basin. Pimentel, N.L.V. carried out detailed sedimentological work on tertiary sequence of Sado Basin in his PhD work “The Sado Tertiary Basin. Sedimentological and tectono-sedimentary analysis” (PhD Thesis, 1997, University of Lisbon). It also includes the work done before in the studied area. We have tried to refine his results by establishing proximal-distal facies, marking different lithostratigraphic units as well as giving more detailed insights into clay minerals variations and their relationship.

2. Framework of the study area

2.1. Location

The study area falls in the southwestern part of Portugal (Fig.1). The Sado Basin is bounded by the Messejana–Plasencia Fault and by two WNW–ESE late Hercynean reactivated faults, the Torrao and Grandola Faults (TF and GF, Fig. 2).

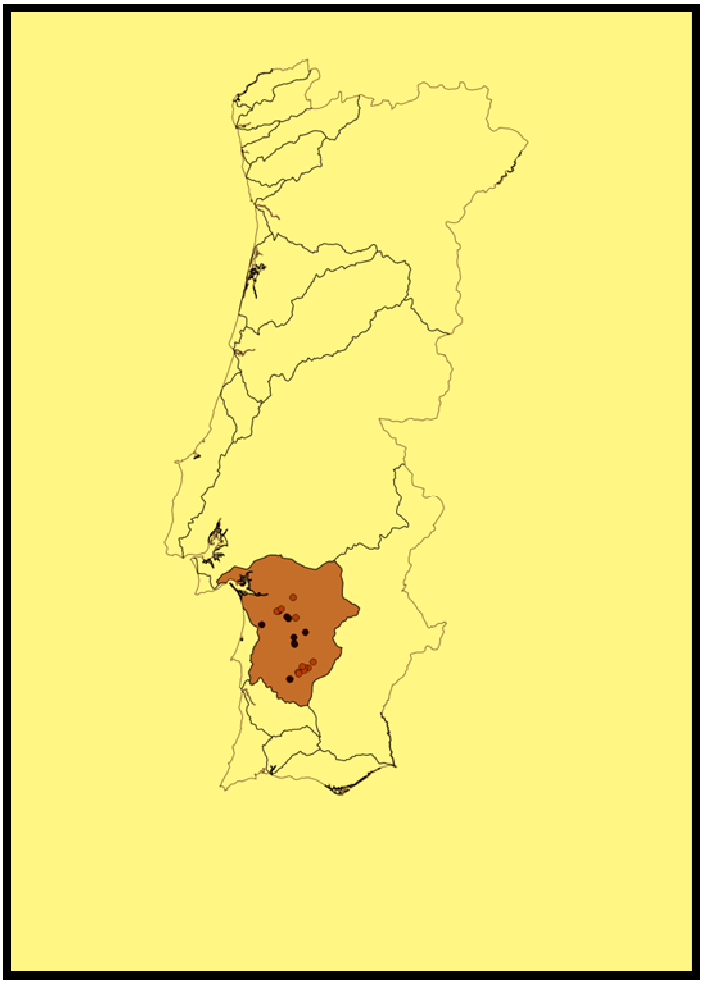

Fig. 1- Location of Sado Basin (in brown) and sampling sites (marked with circles) in Portugal.

2.2. Geology and tectonics

The Sado Basin is a small Tertiary basin, located in the southwestern area of the Iberian Peninsula, which was in connection with the larger Lower Tagus basin (Fig. 2). The formation and tectono-sedimentary evolution of these basins are related to the relative movements between the African and the European lithospheric plates, during the alpine orogeny (Tapponier, 1977; Boillot et al., 1984; Uchupi, 1988; De

Galdeano, 1996). The convergent movement of those plates started in the Palaeocene, leading to intense deformation in the western Mediterranean, but only in the Eocene the compression was transmitted further west into the Iberian Massif. Here, the N–S compression reactivated several originally late Hercynean faults, most of them as NE–SW strike-slip sinistral faults. Several tertiary iberian basins were then formed, such as the Tagus–Sado Basin between the Portuguese Central System and the Messejana–Plasencia Fault (MPF, Fig. 2). The Messejana–Plasencia Fault and the two WNW–ESE late Hercynean reactivated faults (Torrao and Grandola Faults) acted mainly as dip-slip faults, forming a small graben between them, in relation to the first Middle Eocene compressive phases. The sedimentary response was the infilling by thick alluvial fan deposits (Vale do Guizo Formation). During the Oligocene and Early Miocene, with the rotation of the main compression from NE–SW towards E–W (De Galdeano, 1996), subsidence was attenuated and active sedimentation stopped in this basin, restricting the Neogene sedimentary record to less than 40 m of Messinean fluvio-marine deposits and Piacenzian fluvial sands (Pimentel, 1998b). The Neogene deposits lie unconformably and cover most of the Palaeogene, mainly at the SW half of the basin, reducing the outcrops for study. The Palaeozoic basement lies at altitudes between +100 m and -250 m, showing a general dip towards the SW (with several small horsts and grabens), accompanied by an increasing thickness of the Palaeogene sequence, from about 20 m (near the Torrao Fault) to a maximum of 250 m (near the Grandola Fault). There are strong evidences for a syn-sedimentary origin of this dip, namely the presence at the SW border of the Basin of porphyritic basic clasts—with indubitable provenance from the igneous areas forming the footwall of the Torrao Fault to the NE (Pimentel, 2002).

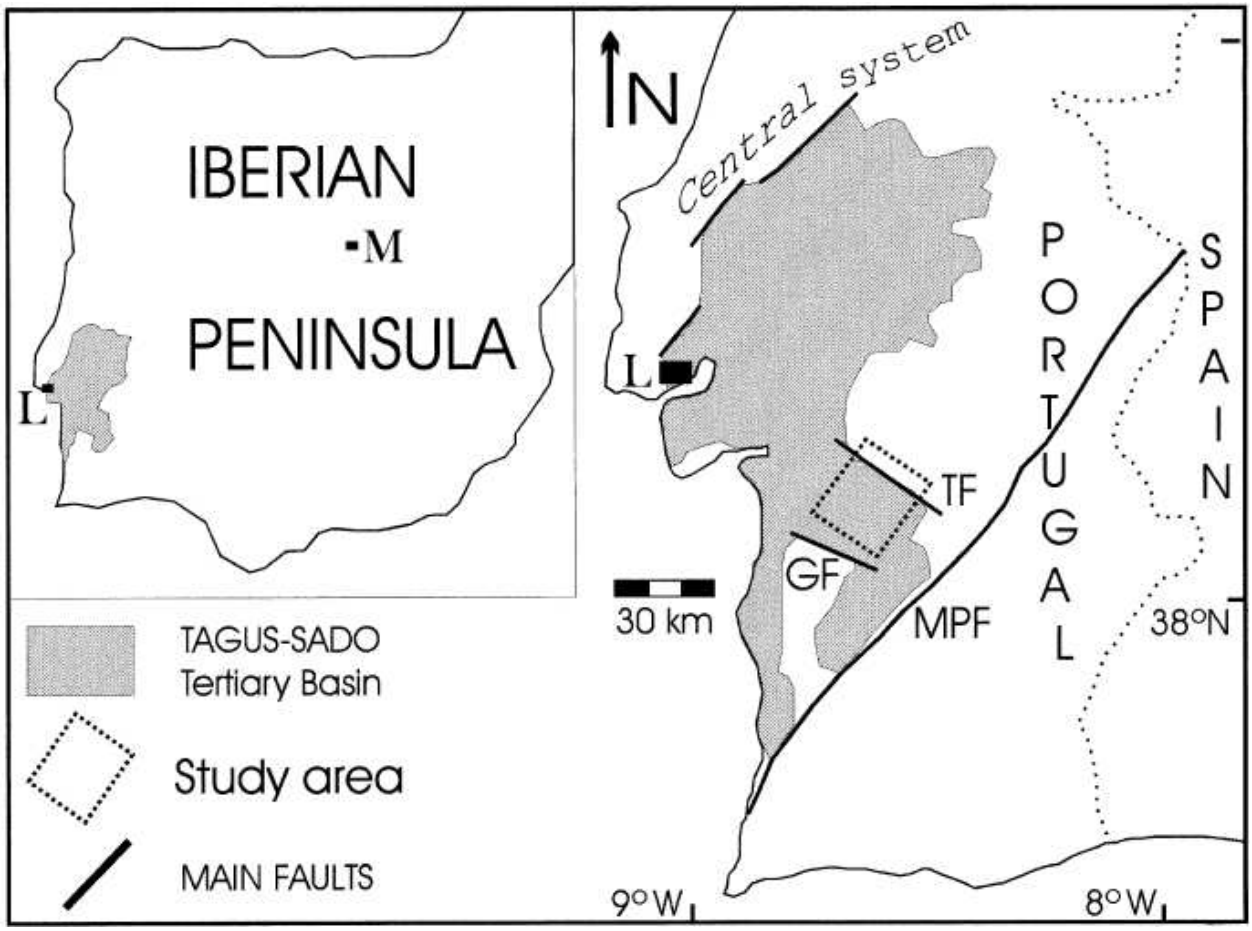

Fig.2- Location of Sado Basin in Iberian Peninsula.

2.3. Climate

According to Köppen (1936) classification, the studied area has temperate climate with warm summer (CSa). A small part of the basin has arid climate (BSk) as shown in the Fig.3 (Instituto português do mar e da atmosfera).

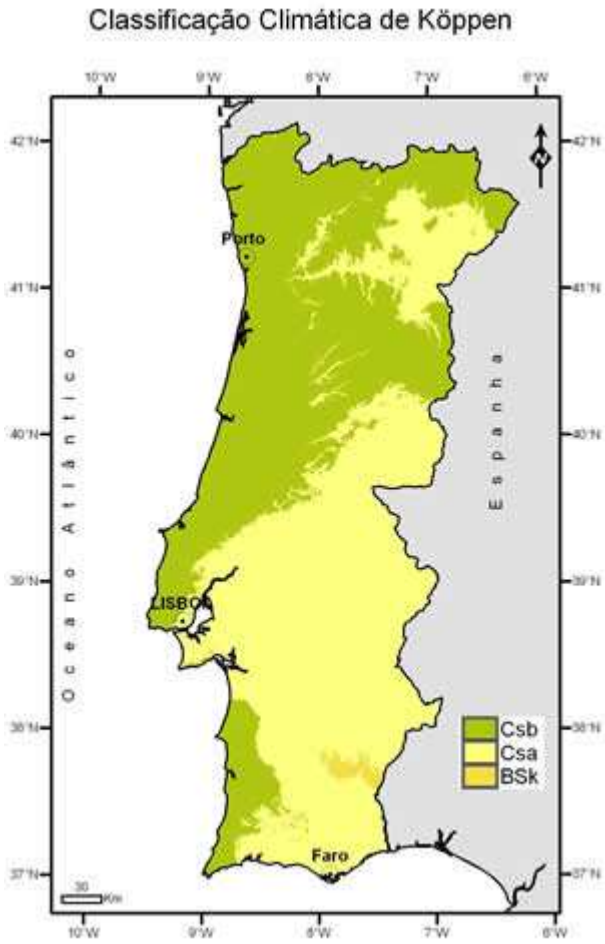

Fig.3- Climate map of Portugal (Csb –temperate climate with dry and warm summer ; Csa –temperate climate with warm summer ; BSk –cold steppe climate).

2.4. Field Work Program

Field work was carried out in two steps. First field campaign was done in order to have a broader view of the area. Second field trip was focused on the sampling of the formations having primarily palygorskite as their main constituents. The present work is based on the field data collected by the field team, comprising the author, technical specialist, Joao Manuel Ferreira Ribeiro and field assistant Mr. Graça under the co-ordinative guidance of Prof. Fernando Tavares Rocha.

2.5. Working Conditions

The study area is very much easy to access through the Motorway. Access to the interior of field study area is very much easy as well. The network of roads in the study area proved to be best access routes for traversing in the investigated area.

3. Sampling and Methodology

This chapter describes the sampling sites and techniques applied for the characterization of samples collected from different parts of Sado basin.

3.1. Sampling

Sampling was carried out in two campaigns. The aim of first campaign was to identify the type and relative amount of clay minerals present in the samples. The second campaign was more focused on fibrous clay minerals found in Formation of Vale do Guizo and Formation of Ervidel.

3.1.1. First Field Campaign

Fig. 4 shows the sampling sites of the collected samples in Sado basin executed in the first campaign. Field photographs for each sample collected during first campaign are given in Fig. 5.

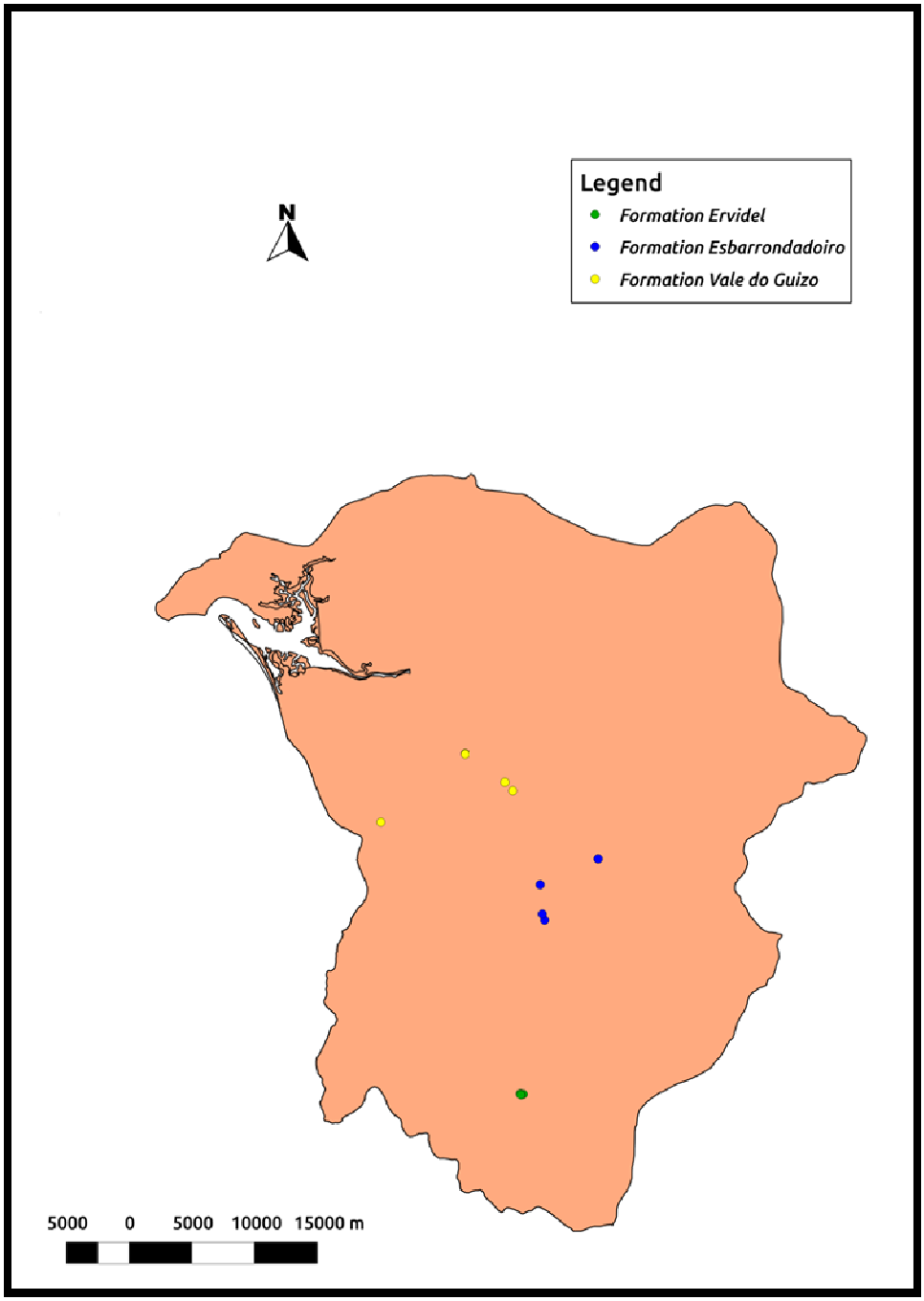

Fig.4- Location of sampling sites in Sado basin during first field campaign.


a)
b)
c)
d)
e)
f)
g)
h)

Fig. 5- Field photographs for samples collected during first field campaign. a) sample S1; b) sample S2 and S3; c) sample S4; d) sample S5; e) sample S6; f) sample S7; g) sample S8; h) sample S9; i) sample S10; j) sample S11; k) sample S12; l) sample S13; m) sample S14.

3.1.2. Second Field Campaign

Field photographs for each sample collected during second campaign for fibrous clay minerals rich formations are given in Fig. 6.


a)
b)
c)
d)
e)
f)
g)
h)

Fig. 6- Field photographs for samples collected during the second field campaign. a) sample SG1; b) sample SG2; c) sample SG3; d) sample SG4; e) sample SG5; f) sample SG6; g) sample SG7; h) sample SG8; i) sample SG9; j) sample SG10; k) sample SG11; l) sample SG12; m) sample SG13; n) sample SG14.

3.2. Methods

This part describes the methods used for the separation and extraction of different sized particles in the laboratory.

3.2.1. Wet sieving

Wet sieving was performed to separate the silt-clay fraction (< 63 μm) from the bulk material. Through the weighting of the obtained fractions, it was also used to assess the particle size distribution of the bulk materials. The method was developed according to the standard test for particle-size analysis of soils (ASTM, 2007). After mixing the bulk sample with distilled water, a #230 washing sieve (63 μm) was placed over a bucket and portions of the suspended sample were transferred to the sieve.

The fine clay was washed through the screen using a squirt bottle, until the wash water was clean. The obtained fractions, silt-clay (< 63 μm) and sand-gravel (> 63 μm), were dried (50^{o}C) and after cooled, they were weighted.

This method was used, rather than dry sieving, because for material that is finer than 150 μm, dry sieving can be significantly less accurate. Wet sieving also produces an adequate degree of separation between individual fractions. Suspending the particles in a suitable liquid allow the transport of fine material through the sieve much more efficiently than shaking the dry material. Furthermore, it allowed the gentle removal of cementing minerals and particles of higher size. These could represent impurities in the material to be studied, compromising its quality.

3.2.2. Sedimentation

Clay fraction was obtained from silt-clay fraction using sedimentation according to Stokes law. The time for particle settling can be calculated using the following equation (Eq. 1):

$$t = \frac{18 \cdot \eta \cdot h}{g \cdot D^2 \cdot (\rho_p - \rho_f)} \quad \text{(Eq. 1)}$$

Where,

t – time, s;

h – height of water column, m;

g – gravitational acceleration, m/s^2;

D – equivalent spherical diameter, m;

ρ_p – mass density of particle, kg/m^3;

ρ_f – mass density of fluid, kg/m^3;

η – dynamic viscosity, kg/m·s.

Table 2 indicates the sedimentation time for a water column of 10 cm and particles equivalent spherical diameter 2 μm for different temperatures.

Table 2- Time and temperature for 2 μm particles sedimentation.

Temperature, ^{o}C	Time, hh:mm:ss
15	8:47:39
16	8:33:42
17	8:20:41
18	8:08:07
19	7:56:02
20	7:44:24
21	7:33:13
22	7:22:03
23	7:11:48
24	7:01:34
25	6:52:15

The sedimentation procedure was carried out as follows: 20 grams of dried less than 63 μm fraction was suspended in 1000 ml of distilled water using ultra-sound and passed to cylinders (illustrated in Fig. 7). The uppermost 10 cm column of suspension was collected after a time period as given in the above table. When necessary, antifloculant was added to the suspension. Then, the collected suspension was put in the stove to dry at 50^{o}C. The procedure was performed several times until the water became clean or the necessary amount of the less than 2μm fraction was obtained. The dried sample was grinded in agate mortar and stored for further analyses.

Fig.7- Cylinders used for sedimentation.

3.2.3. Mineralogical analysis

3.2.3.1. X-ray diffraction

Crystalline phases in samples were determined using X-ray diffractometer (XRD). Powder x-ray diffractogram was obtained for fraction < 63 μm. Clay fraction was characterized by preparing oriented slides, which were later treated with glycerol and heated for 500^{o} C. The scanning was performed form 4^{o} to 65^{o} 2Θ, step 0,02^{o}, scanning speed 0,02^{o}/s. Sample was analysed using X'Pert-Pro MPDPhilips/PANalytical X-ray diffractometer (CuKα; λ = 1.5405 Å) operating at 50 kV and 30 mA. In the case of clay fraction the scanning was performed from 4^{o} to 20^{o}. The identification and semi-quantification of peaks was done manually using recommendations and given data of Brindley and Brown (1980).

3.2.3.2. Scanning electron microscope

Scanning electron microscopy (SEM) is a useful technique to study mineralogical and textural composition of clay minerals. SEM was used to ascertain the minerals found in diffractograms. It was also applied to ascertain the chemical composition of specific mineral phases.

The parameters, which influence the image quality are accelerating voltage, beam current and probe current, Bias voltage, working distance, spot size, diaphragm size and aperture (Brisset, 2008). In our study, we used a Hitachi S-4100 Scanning Electron Microscope. Operating voltage was 25kV and working distance

15 mm, carbon coating was applied to the samples to enhance the electron emission from their surface.

3.2.4. Chemical analysis

3.2.4.1. X-ray fluorescence spectroscopy

Chemical analysis for less than 63 μm fraction was performed using X-ray fluorescence spectroscopy (XRF). Preparation of sample included the mixture of 10 g of sample with 5 drops of 2% Mowiol® (commercial product of polyvinyl alcohol) to improve adhesion and then pressure into platelet applying 15 T of pressure for 40 seconds. Analysis was performed with XRF AxiosPANalytical spectrometer equipped with Rh bulb, the gas used - Argon/Methane, data processing program – IQ+ (major elements) and Pro-Trace (minor elements). For complete chemical analysis loss of ignition (LOI) was also determined by heating 1g of the sample at 1000^{o} C for 1 hour in furnace.

3.2.4.2. Energy dispersive X-ray spectroscopy

Energy dispersive X-ray spectroscopy (EDS) was applied to study elemental analysis for minerals observed in SEM. It allowed us to confirm the type of mineral and to calculate its chemical formula. In case of doubts, it helped to identify the possible mineral, studying the obtained chemical analysis. The same Hitachi S-4100 microscope as for SEM analysis was used for EDS analysis.

4. Results

The results obtained are divided into Results (I) and Results (II) according to two field campaigns done, respectively.

4.1. Results (I)

These results present the characterization of samples S1 to S14.

4.1.1. Mineralogical characterization (I)

The mineralogical phases present in the samples from S1 to S14 were identified from Powder X-rays diffractograms and semi-quantification was done manually according to the recommendations of Brindley and Brown (1980). The results are given in the Table.2

Table 2- Mineralogical composition of samples (S1 to S14) collected in Sado basin during the first field campaign.

Epoch	Formation	Sample No.	Mineralogical Composition %									
			Phyllosilicates	Quartz	K-Feldspar	Plagioclase	Opal	Calcite	Dolomite	Siderite	Hematite	Pyrite
Miocene	Esbarrondadoiro	S5	67	23	9			2				
		S6	70	5	4	19					1	
		S7	78	9	8	4						
		S8	74	15	5	2				4		
		S9	16	42	19	15	3	3	2			
Eocene	Ervidel	S1	57	12	6	14		4	6		2	
		S2	55	13	6	11		8	5		2	
		S3	51	15	4	1		16	5	2	3	4
		S4	57	13		15	8			2	5	
	Vale do Guizo	S14	71	11	10	7				1		
		S13	59	9	7	17	8					
		S12	68	7		8	17					
		S11	55	22	6	15				2		
		S10	83	6	5	6						

The graphical representation of these results is given in Fig. 8.

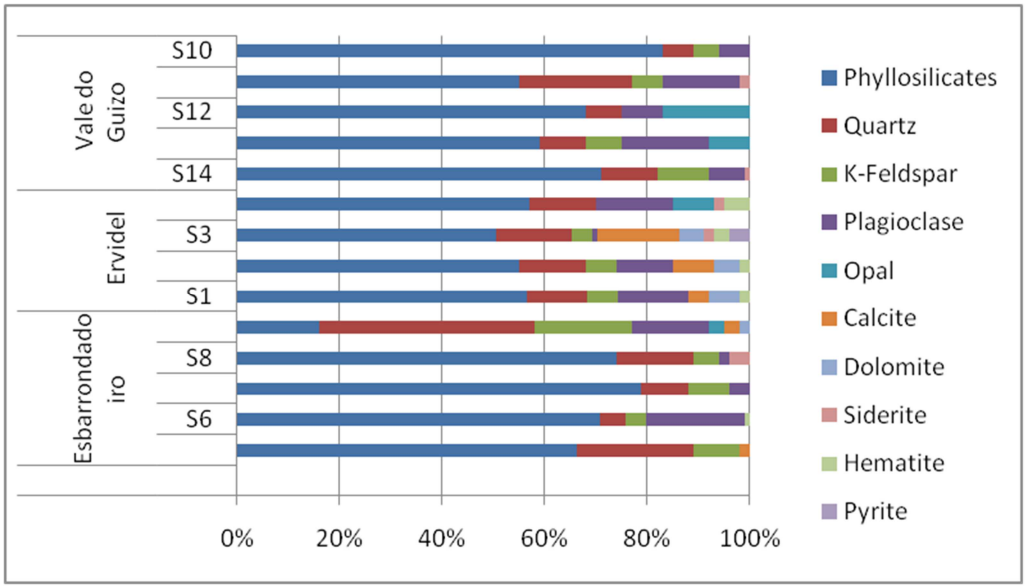

Fig. 8- Mineralogical composition of samples (S1 to S14) collected in Sado basin during the first field campaign.

The clay minerals namely palygorskite, smectite, illite, chlorite, kaolinite, kaolinite/smectite (KS) mixed layer were identified from oriented and treated slides by XRD. The quantitative results for samples S1 to S14 are given along with Kubler Index as in Table 3.

Table 3- Clay minerals composition of samples (S1 to S14) collected in Sado basin during the first field campaign.

Epoch	Formation	Sample No.	Clay Minerals Composition %						Kubler.I
			Palygorskite	Smectite	Illite	Chlorite	Kaolinite	KS	
Miocene	Esbarrondadoiro	S5			7		93		1.5
		S6			98			2	2.0
		S7			7		93		1.5
		S8		3	20		77		2.5
		S9			32		68		1.5
Eocene	Ervidel	S1	67	3	17		13		3.0
		S2	62	2	23		13		2.0
		S3	64	4	22		10		4.0
		S4	76	2	16		6		3.0
	Vale do Guizo	S14	32	30	28		10		3.0
		S13	56	20	16		8		4.0
		S12			46	32	13	10	7.0
		S11			28	2	70		4.0
		S10			9		91		2.0

The graphical representation of the clay minerals results are given in Fig. 9.

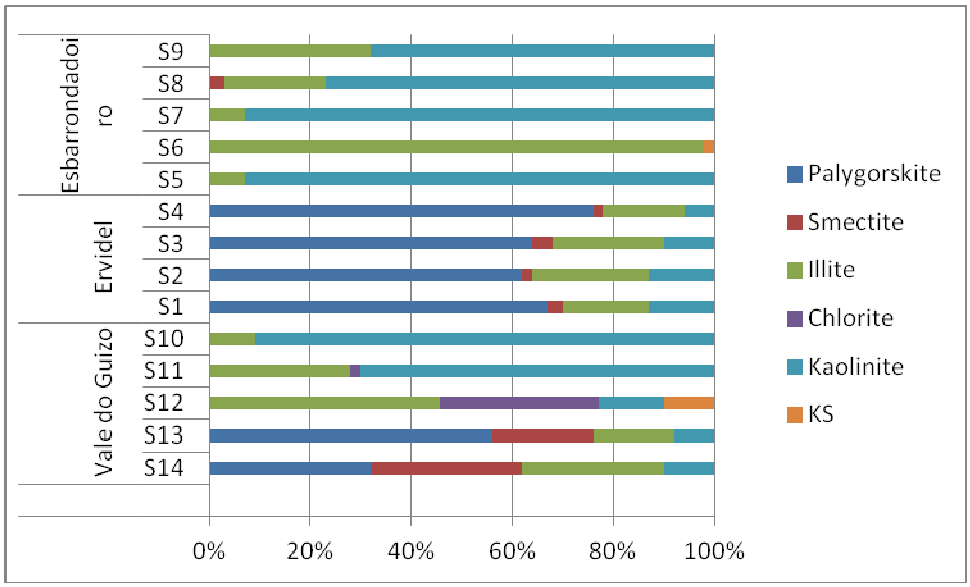

Fig. 9- Clay minerals composition of samples (S1 to S14) collected in Sado basin during the first field campaign.

4.1.2. Chemical characterization (I)

Chemical results (major elements) obtained from XRF are tabulated below for samples S1 to S14 (Table 4).

Table 4- Chemical composition of samples (S1 to S14) collected in Sado basin during the first field campaign.

Epoch	Formation	Sample No.	Chemical Composition %										
			LOI	Na2O	MgO	Al2O3	SiO2	P2O5	SO3	K2O	CaO	TiO2	Fe2O3
Miocene	Esbarronda-doiro	S5	8.0	0.1	0.6	25.4	58.5	0.1	0.1	1.5	0.2	0.7	4.7
		S6	10.8	0.1	0.7	29.6	49.2	0.1	0.1	1.5	0.1	0.4	7.2
		S7	11.5	0.2	0.6	28.4	47.7	2.3	0.1	1.3	0.0	0.5	7.0
		S8	10.2	0.2	0.8	25.2	52.5	0.0	0.0	1.6	0.2	0.9	8.4
		S9	0.7	0.4	0.2	8.9	84.6	0.1	0.0	2.3	0.2	0.9	1.6
Eocene	Ervidel	S1	12.4	0.1	**6.5**	16.4	54.3	0.1	0.1	1.6	**2.4**	0.5	5.6
		S2	10.3	0.2	**5.3**	16.1	55.7	1.3	0.0	1.5	**3.8**	0.6	5.0
		S3	15.2	0.4	**3.7**	14.9	52.1	0.2	0.1	1.5	**6.7**	0.6	4.6
		S4	13.8	0.2	**5.8**	16.7	52.8	0.0	0.0	1.5	**3.8**	0.6	4.7
	Vale do Guizo	S14	7.4	0.3	**4.4**	18.6	57.2	1.9	0.0	2.0	**0.9**	0.8	6.2
		S13	6.5	0.2	**4.1**	20.2	59.0	1.5	0.0	1.6	**1.3**	0.5	5.0
		S12	9.8	0.5	1.3	26.4	50.6	0.1	0.1	1.7	0.5	0.5	8.2
		S11	6.4	0.2	0.4	21.0	63.8	0.1	0.0	2.9	0.1	0.7	4.3
		S10	12.5	0.1	0.3	32.0	46.5	0.1	0.1	1.6	0.1	0.2	6.4

Note: LOI-Loss on ignition.

4.2. Results (II)

In this part, results from second campaign are presented. These samples were collected from two formations, Formation of Ervidel and Formation of Vale do Guizo which are the most rich in Palygorskite.

4.2.1. Mineralogical characterization (II)

The mineralogical associations present in the samples from SG1 to SG14 were identified from Powder X-rays diffractograms and semi-quantification was done manually according to the recommendations of Brindley and Brown (1980), the same way as done for samples SG1 to SG14. The results are given in the Table 5.

Table 5- Mineralogical composition of samples (SG1 to SG14) collected in Sado basin during the second field campaign.

Formation	Sample	Mineralogical Composition %											
		Phy.	Quartz	K-Feldspar	Plag.	Opal	Anatase	Calcite	Dolomite	Hematite	Pyrite	Anhydrite	Magnesite
Ervidel	SG1	38	5	4	20	8	9	12	3	2			
	SG2	44	7	4	8			30	3	1	2		
	SG3	42	12		17	13			13	4			
	SG4	71	21		4				3			2	
	SG5	50	15		17	5			4	1	2		
	SG6	62	8	6	14	7				1	1		1
	SG7	67	18		4	7				2	3		
Vale do Guizo	SG8	47	12	4	4				32	1			
	SG9	48	10						37	3	2		
	SG10	47	9		9	6			27	2			
	SG11	78	6		10		6						
	SG12	75	9		14				2				
	SG13	56	4		13			17		1	1		8
	SG14	72	6		13	6							

Note: Phy – phyllosilicates; Plag – Plagioclase.

The graphical representation of these results is given in Fig. 10.

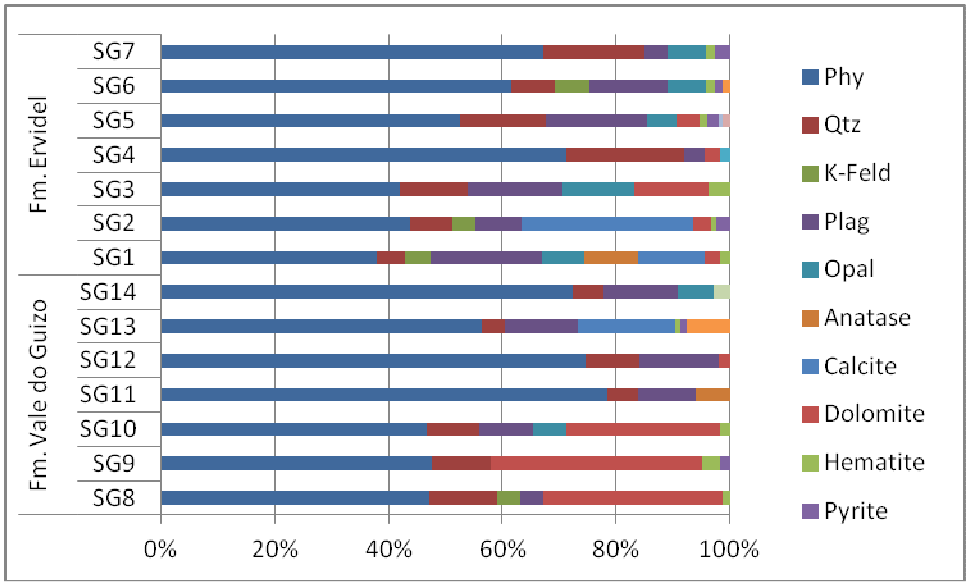

Fig. 10- Mineralogical composition of samples (SG1 to SG14) collected in Sado basin during the second field campaign.

The clay minerals including palygorskite, smectite, illite, chlorite, kaolinite, kaolinite/smectite (KS) mixed layer and chlorite/smectite (CS) mixed layer were identified from oriented and treated X-rays slides. The quantitative results for samples SG1 to SG14 are given along with Kubler Index as in Table 6.

Table 6- Clay minerals composition of samples (SG1 to SG14) collected in Sado basin during the second field campaign.

Epoch	Formation	Sample	Clay Minerals Composition %							
			Palygorskite	Smectite	Illite	Chlorite	Kaolinite	CS	KS	Kubler.I
Eocene	Ervidel	SG1	76	5		19				
		SG2	73	3	15	9				4.0
		SG3	70		16		8	5		3.0
		SG4		24	47		29			4.5
		SG5	69		18		9	4		4.0
		SG6	90		10					4.0
		SG7			32			38	30	2.0
	Vale do Guizo	SG8	32	9	18	35	6			5.0
		SG9	59	10	10	18	3			4.0
		SG10	61	8	10	20	1			4.0
		SG11	75	21					4	
		SG12	65	8	8	19	1			3.0
		SG13	85	3	12					4.0
		SG14	24	65	5		6			2.0

Note : CS- Chlorite/Smectite, KS- Kaolinite/Smectite.

The graphical representation of these results is given in Fig. 11.

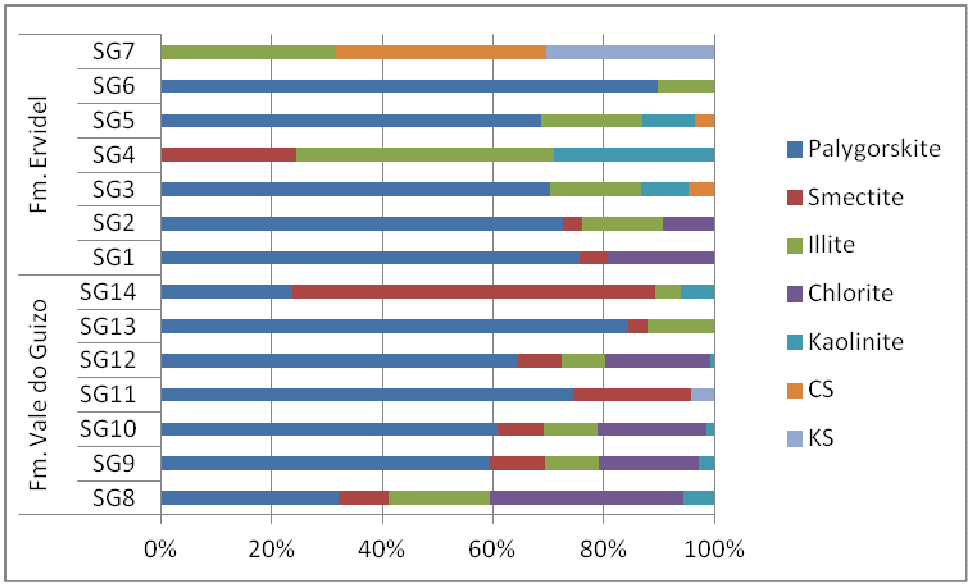

Fig. 11- Clay minerals composition of samples (SG1 to SG14) collected in Sado basin during the second field campaign.

4.2.2. Chemical characterization (II)

Chemical results (major elements) obtained from XRF are tabulated below for samples SG1 to SG14 (Table 7).

Table 7- Chemical composition of samples (SG1 to SG14) collected in Sado basin during the second field campaign.

Epoch	Formation	Samples	Chemical Composition %											
			LOI	Na2O	MgO	Al2O3	SiO2	P2O5	SO3	Cl	K2O	CaO	TiO2	Fe2O3
Eocene	Ervidel	SG1	13.1	0.8	7.9	13.5	46.5	0.2	0.1	0.0	0.3	4.9	1.9	10.7
		SG2	21.5	0.1	5.4	12.8	44.4	0.0	0.0	0.0	0.8	10.7	0.4	3.7
		SG3	13.6	0.5	5.7	16.4	52.8	0.0	0.1	0.4	1.2	4.1	0.4	4.7
		SG4	7.6	0.3	1.0	20.1	62.6	0.0	0.1	0.0	1.7	0.0	0.6	5.8
		SG5	9.6	0.3	4.6	18.6	55.8	2.1	0.0	0.0	1.8	0.3	0.7	5.9
		SG6	12.4	0.2	7.4	12.4	60.7	1.4	0.2	0.0	0.6	0.1	0.4	4.2
		SG7	9.6	0.4	2.3	19.9	59.0	0.0	0.3	0.0	1.3	0.3	0.7	6.1
	Vale do Guizo	SG8	20.3	0.2	5.8	14.0	44.7	0.0	0.1	0.0	1.2	9.1	0.6	3.8
		SG9	29.3	0.1	9.1	9.6	32.6	0.0	0.1	0.0	0.7	15.6	0.3	2.3
		SG10	26.3	0.2	8.0	10.7	39.0	0.0	0.1	0.0	0.8	11.7	0.4	2.7
		SG11	13.0	0.3	3.6	24.0	53.4	0.0	0.1	0.1	1.0	0.7	0.4	3.3
		SG12	11.6	0.7	6.1	16.1	55.3	0.0	0.5	1.0	1.4	0.8	0.7	5.5
		SG13	20.4	0.1	4.3	15.6	45.4	0.0	0.0	0.0	0.6	9.7	0.3	3.4
		SG14	10.1	0.2	2.8	22.2	54.5	1.6	0.2	0.0	0.9	1.1	0.6	5.4

Note : LOI- Loss on ignition

4.2.3. Crystallochemical characterization

The crystallochemical formulas obtained from EDX-SEM analysis for palygorskite are given in the following table (Table 8).

Table 8- Crystallochemical composition of palygorskite rich samples.

Formation	Sample No.	Si	Al IV	ΣT	Mg	Al IV	Fe	Ti	ΣO	Ca	K	Na
Fm. Ervidel	SG1	7.70	0.30	8.00	0.34	3.28	0.27	0.20	4.09		0.54	
		7.68	0.32	8.00	1.50	2.07	0.78		4.35	0.08	0.01	
		8.00		8.00	1.30	2.38	0.46		4.14			0.32
		8.00		8.00	0.97	1.92	1.26	0.08	4.23	0.13	0.03	
	SG2	7.77	0.23	8.00	1.05	2.89	0.37		4.31	0.13		
	SG5	6.08	1.92	8.00	1.16	1.78	1.22		4.16		0.62	
		6.55	1.45	8.00	1.02	1.42	1.34	0.09	3.87		0.57	
		6.34	1.66	8.00	0.93	1.53	1.40	0.19	4.05		0.72	
	Mean Value	7.27	0.74	8.00	1.03	2.16	0.89	0.07	4.15	0.04	0.31	0.04
Fm. Vale do Guizo	SG8	7.00	1.00	8.00	1.26	1.91	0.57	0.05	3.79		0.26	0.61
		6.81	1.19	8.00	0.89	1.67	1.20	0.10	3.86		0.50	
		7.05	0.95	8.00	0.83	1.69	1.20	0.08	3.80		0.51	
		7.17	0.83	8.00	0.90	1.89	0.92	0.06	3.77		0.45	
	SG9	7.01	0.99	8.00	1.09	1.79	0.90	0.12	3.90		0.39	
		6.99	1.01	8.00	1.17	1.88	0.83	0.07	3.95		0.37	
		7.10	0.90	8.00	1.12	1.82	0.85	0.09	3.88		0.36	
	SG11	7.21	0.79	8.00	0.72	2.54	0.36	0.05	3.67	0.13	0.26	
		6.99	1.01	8.00	0.76	2.88	0.24		3.88		0.14	
		6.81	1.19	8.00	0.68	2.71	0.46		3.85	0.08	0.20	
		6.94	1.06	8.00	0.79	2.42	0.58		3.79	0.17	0.15	
	SG13	8.00		8.00	0.88	1.87	0.26		3.01	0.11	0.09	
	Mean Value	7.09	0.91	8.00	0.92	2.09	0.70	0.05	3.76	0.04	0.31	0.05

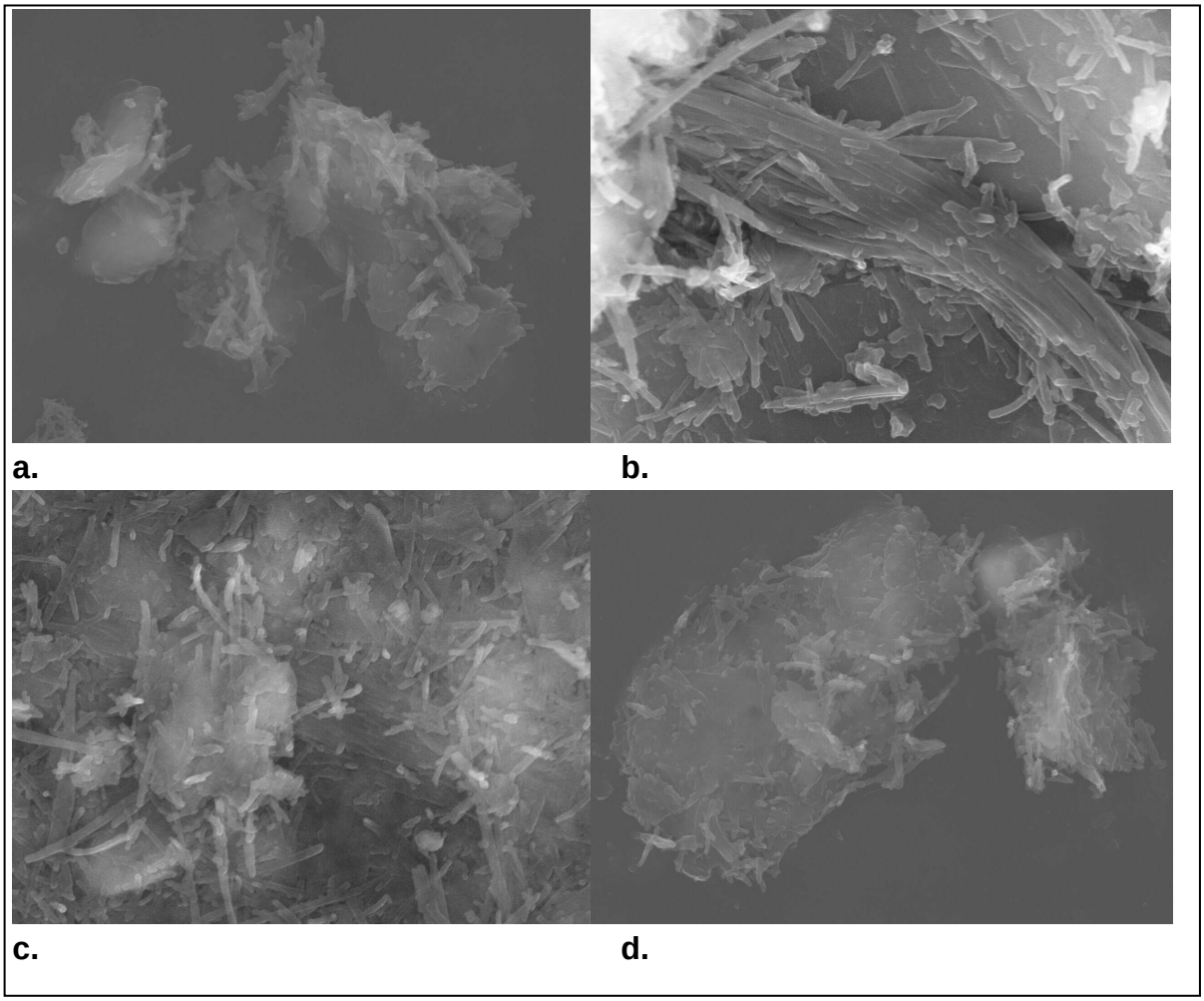

Fig.12- SEM images showing palygorskite fibers. a. and b. sample SG1; c. and d. sample SG2.

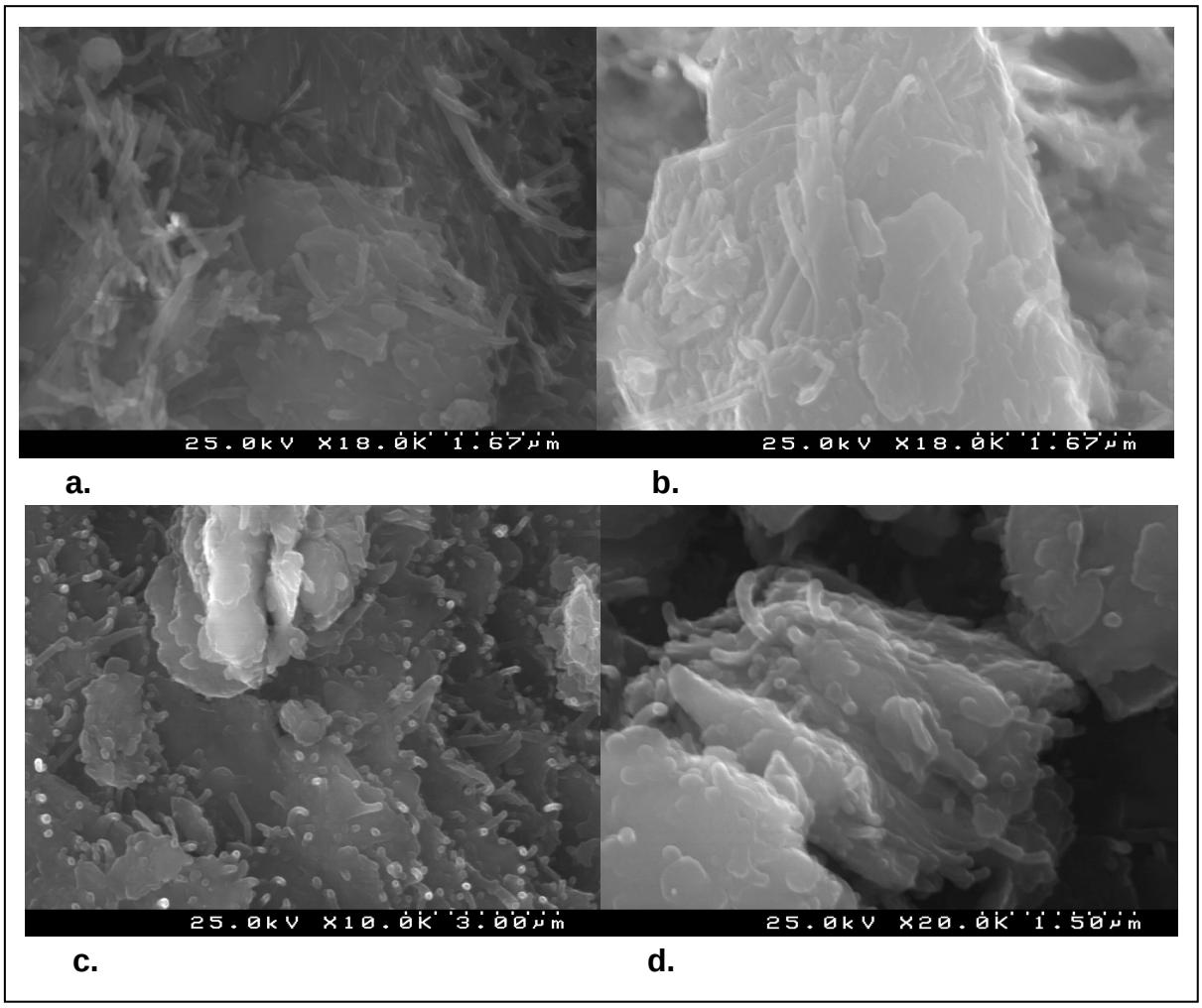

Fig. 13-SEM images showing palygorskite fibers. a. and b. sample SG5; c. and d. sample SG8.

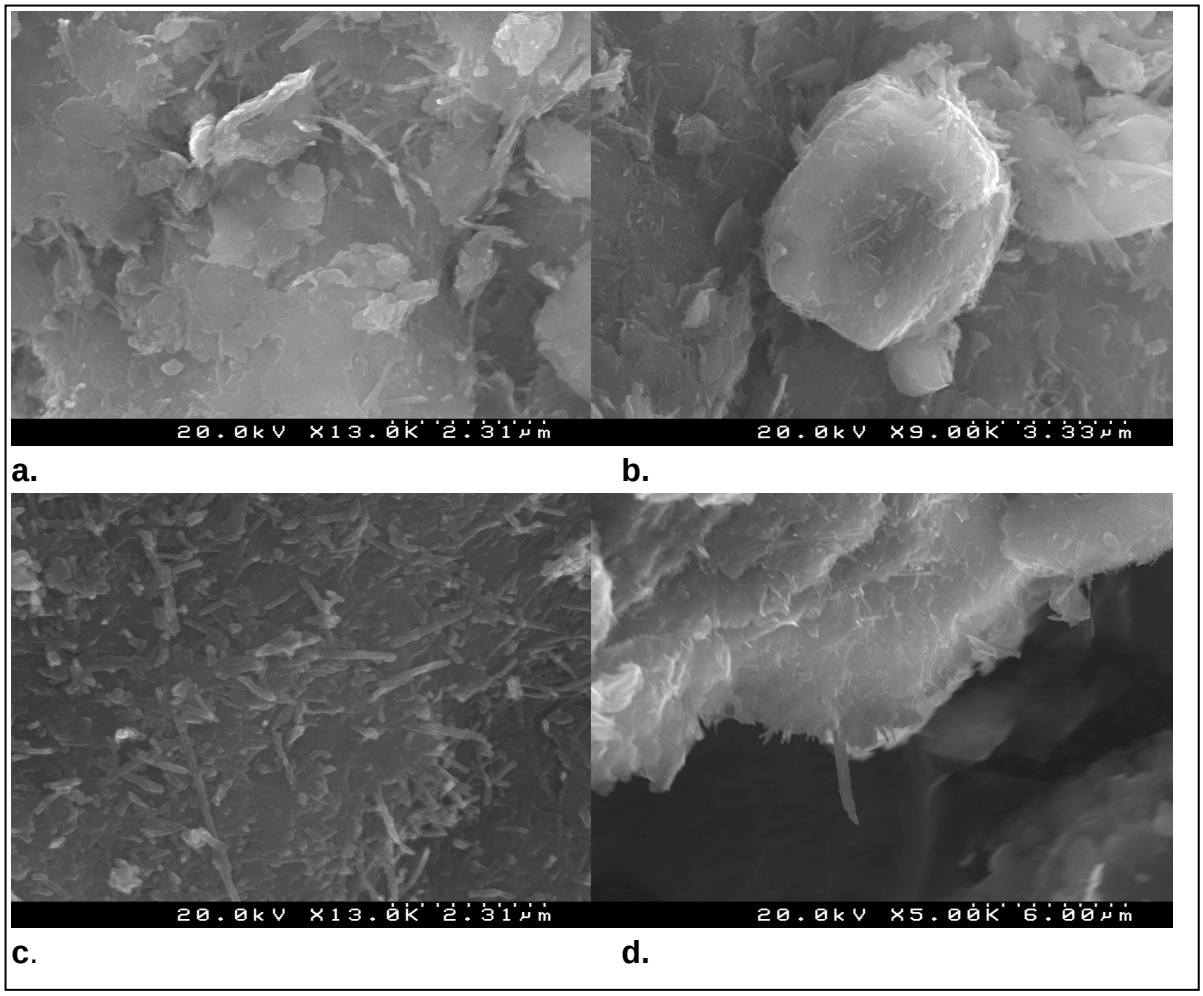

Fig.14- SEM images showing palygorskite fibers. a. and b. sample SG9; c. and d. sample SG11.

5. Discussion and Conclusion

The results obtained from XRD, XRF and SEM-EDS analyses are discussed in two parts as following:

1. Lithostratigraphic markers
2. Paleoenvironmental reconstruction and diagenesis

5.1. Lithostratigraphic markers

One major application of clay minerals in basin analysis consists of the utilization of selected minerals as lithostratigraphic markers allowing the definition of guide-layers in field sections or in borehole logs. These guide-layers are established on the basis of clear anisotropies found out in the lateral or vertical evolution of the selected mineralogical parameters. The use of clay minerals as lithostratigraphical markers can be announced like a fossil, a mineral or an association of minerals can characterize a layer and allow regional correlations (Pomerol, 1987).

According to Results (I), formation of Esbarrondadoiro can be divided into two units based on bulk sample analysis and clay size fraction analysis.

1. Formation of Esbarrondadoiro Unit (I). This unit (samples S5, S6, S7, S8) consists of phyllosilicate + quartz + K-feldspar + plagioclase. In the clay size fraction, this unit is characterized by the clay mineral assemblage of kaolinite + illite with very minor amounts of smectite and mixed layers KS.
2. Formation of Esbarrondadoiro Unit (II). This unit (sample S9) consists of less phyllosilicate + high quartz + high K-feldspar + high plagioclase + small amount of opal, calcite and dolomite. In clay size fraction, this unit can be distinguished with the more proportional ratio of kaolinite and illite minerals.

Table 9- Mineralogical composition of samples from Formation of Esbarrondadoiro.

Formation	Sample No.	Mineralogical Phases Composition %									
		Phy.	Quartz	K-Feldspar	Plag.	Opal	Calcite	Dolomite	Siderite	Hematite	Pyrite
Esbarrondadoiro	S5	67	23	9			2				
	S6	70	5	4	19					1	
	S7	78	9	8	4						
	S8	74	15	5	2				4		
	S9	16	42	19	15	3	3	2			

The bulk samples results obtained from Results (I) and (II) for Formation of Ervidel show also a possible division into two units.

1. Formation of Ervidel Unit (I). It contains phyllosilicate + quartz + K-feldspar + plagioclase + opal + carbonates (calcite/dolomite) with minor amount of hematite/pyrite. The samples (S1, S2, S3, SG1, SG2 and SG3) are relatively poor in phyllosilicate and rich in carbonates >10% (calcite or/and dolomite).

2. Formation of Ervidel Unit (II). This unit consists of samples (S4, SG4, SG5, SG6 and SG7) which are relatively richer in phyllosilicate, they are very poor in carbonates.

Table 10- Mineralogical composition of samples from Formation of Ervidel.

Formation	Sample	Mineralogical Composition %											
		Phy.	Quartz	K-Feldspar	Plag.	Opal	Anatase	Calcite	Dolomite	Hematite	Pyrite	Anhydrite	Magnesite
Ervidel	S1	57	12	6	14			4	6		2		
	S2	55	13	6	11			8	5		2		
	S3	51	15	4	1			16	5	2	3	4	
	S4	57	13		15	8				2	5		
	SG1	38	5	4	20	8	9	12	3	2			
	SG2	44	7	4	8			30	3	1	2		
	SG3	42	12		17	13			13	4			
	SG4	71	21		4				3			2	
	SG5	50	15		17	5			4	1	2		
	SG6	62	8	6	14	7				1	1		1
	SG7	67	18		4	7				2	3		

Note: Phy – phyllosilicates; Plag – Plagioclase.

In clay size fraction, this formation contains palygorskite, illite, smectite, chlorite, kaolinite and mixed layers KS or/and CS.

The bulk sample analysis (from Results(I) and (II)) reveals that Formation of Vale do Guizo consists of phyllosilicate, quartzs, K-feldspar, plagioclase, varying content of carbonates (calcite, dolomite) with minor amount of opal, anatase, hematite, pyrite and magnesite in some samples. Based on mineralogical associations, two units are distinguished here as following:

1. Formation of Vale do Guizo Unit (I). The samples (S10, S11, S12, S13, SG11, SG12 and SG14) are relatively rich in phyllosilicate and poor in terms of carbonates.
2. Formation Vale do Guizo Unit (II). The samples (SG8, SG9, SG10 and SG13) are relatively rich in carbonates (calcite or/and dolomite) and poor in phyllosilicate.

In clay size fraction, Formation of Vale do Guizo contains palygorskite, smectite, chlorite, illite, kaolinite with small quantity of mixed layer KS.

Table 11- Mineralogical composition of samples from Formation of Vale do Guizo.

Formation	Sample	Mineralogical Composition %											
		Phy.	Quartz	K-Feldspar	Plag.	Opal	Anatase	Calcite	Dolomite	Hematite	Pyrite	Anhydrite	Magnesite
Vale do Guizo	S14	71	11	10	7					1			
	S13	59	9	7	17	8							
	S12	68	7		8	17							
	S11	55	22	6	15					2			
	S10	83	6	5	6								
	SG8	47	12	4	4				32	1			
	SG9	48	10						37	3	2		
	SG10	47	9		9	6			27	2			
	SG11	78	6		10		6						
	SG12	75	9		14				2				
	SG13	56	4		13			17		1	1		8
	SG14	72	6		13	6							

Note: Phy – phyllosilicates; Plag – Plagioclase.

The crystallinity of illite (Kubler index) can be used to demarcate the lithostratigraphic boundaries between these three formations.

Table 12- Kubler index and Biscaye's index of samples from Formations of Esbarrondadoiro, Ervidel and Vale do Guizo.

Formation	Sample No.	Kubler Index	Biscaye's Index
Esbarrondadoiro	S5	1.5	
	S6	2.0	
	S7	1.5	
	S8	2.5	1.0
	S9	1.5	
	Mean Value	**1.8**	**1.0**

Table 13- Kubler index and Biscaye's index of samples from Fm. Ervidel

Formation	Sample No.	Kubler Index	Biscaye's Index
Ervidel	S1	3.0	1.2
	S2	2.0	1.1
	S3	4.0	1.1
	S4	3.0	1.2
	SG1		1.2
	SG2	4.0	1.1
	SG3	3.0	1.3
	SG4	4.5	1.1
	SG5	4.0	
	SG6	4.0	
	SG7	2.0	1.2
	Mean Value	**3.4**	**1.1**

Table 14- Kubler index and Biscaye's index of samples from Fm. Vale do Guizo

Formation	Sample No.	Kubler Index	Biscaye's Index
Vale do Guizo	S14	3.0	1.2
	S13	4.0	1.1
	S12	7.0	
	S11	4.0	
	S10	2.0	
	SG8	5.0	1.0
	SG9	4.0	1.4
	SG10	4.0	1.3
	SG11		1.1
	SG12	3.0	1.2
	SG13	4.0	1.4
	SG14	2.0	1.1
	Mean Value	**3.8**	**1.2**

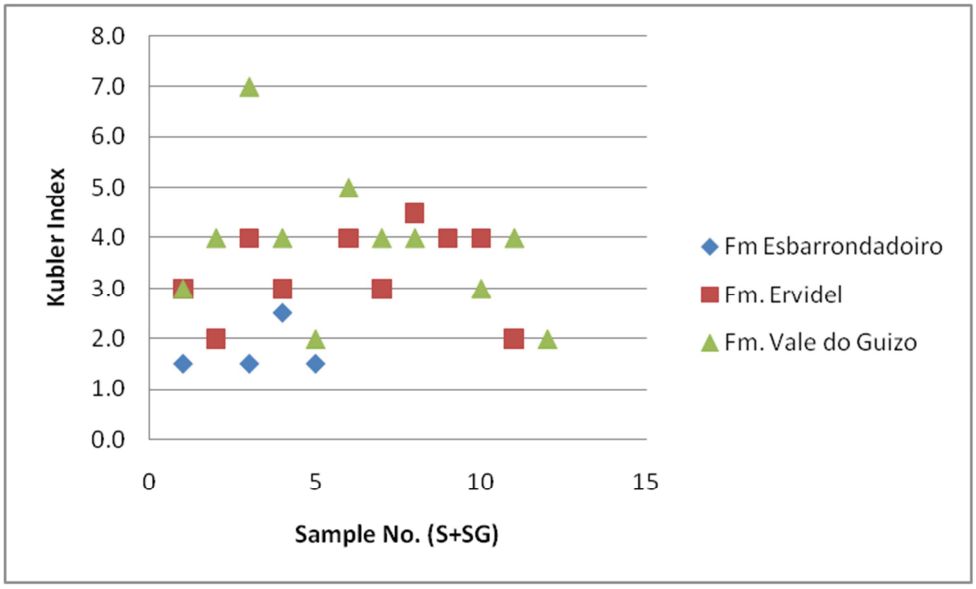

Fig. 15- Kubler index determined for samples collected in the three formations, Sado basin.

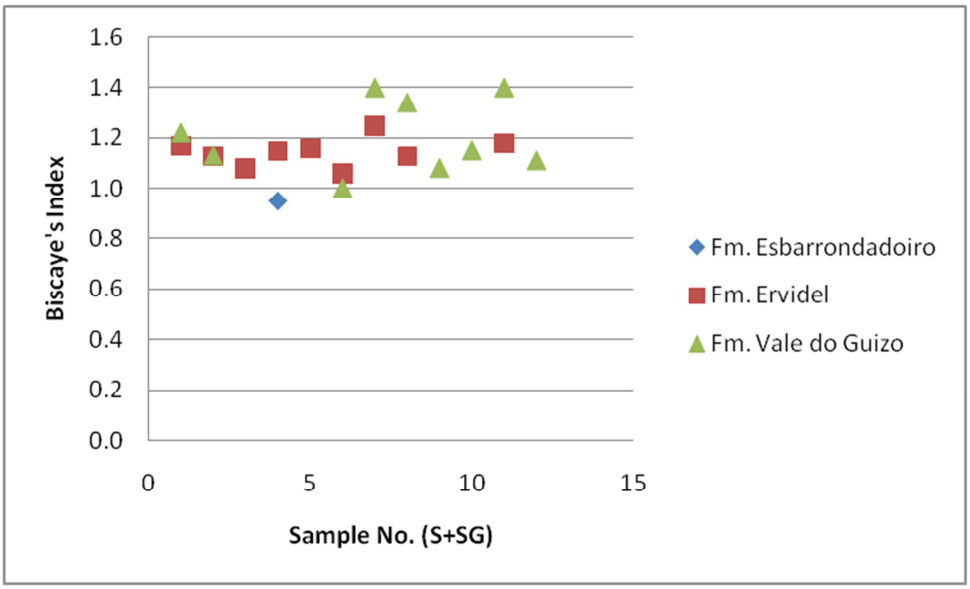

Fig.16- Biscaye's index determined for samples collected in the three formations from Sado basin.

The mean value for Kubler index and Biscaye's Index increases downward with the chronological order (Table 1). The younger Miocene formation, Formation of Esbarrandodairo has the least mean Kubler index value (1.8) whereas the more older formations, Formations of Ervidel and Vale do Guizo have the mean Kubler index values of 3.4 and 3.8 respectively showing that there are more diagenetic imprints on the older formations.

5.2. Paleoenvironment

A schematic sedimentary model for palygorskite formation is given in Figure 17 that shows a cross section where the transition from an alluvial fan environment to a palustrine–lacustrine one can be observed, taking into account the presence of a source area comprised igneous and metamorphic rocks and the interaction of three water types: groundwater, runoff and lacustrine water. The rocky substrate of the parent area is fundamental in order to justify inputs of Mg or Si. The silica input can come from any magmatic rock, particularly those with a felsic composition, or from silica-rich metamorphic rocks and siliciclastic or biosiliceous (diatomite) sedimentary rocks. The Mg source can be any type of rock containing Mg-rich minerals, including magmatic rock (basalt, gabbro and peridotite), metamorphic rock (slate, serpentinite) or sedimentary rock (dolomite, magnesite and magnesian clays). The Si and Mg released in these zones can travel distances and accumulate in flooded lacustrine zones. Given its low solubility except with very alkaline pH levels, aluminium will tend to be less mobile and remain in the vicinity

of its parent rock area, or it may be transported as sediment in aluminous clay particles or colloids. Phenomena occurring in the parent rock area can favour the formation of aluminous clay minerals and the release of Mg and Si, which would favour palygorskite formation in lacustrine conditions, mainly by transformation. Detrital aluminous clay minerals are abundant in distal alluvial fan facies. Palygorskite may be formed there as the result of the transformation of the inherited aluminous clays in the vicinity of a lacustrine environment, particularly during periods of exposure. This process favours calcite precipitation. In areas nearest to a lake, more specifically in the zone containing intertidal mudflats where the water is more alkaline, the transformation of aluminous smectite into saponite would be favoured instead of forming palygorskite.

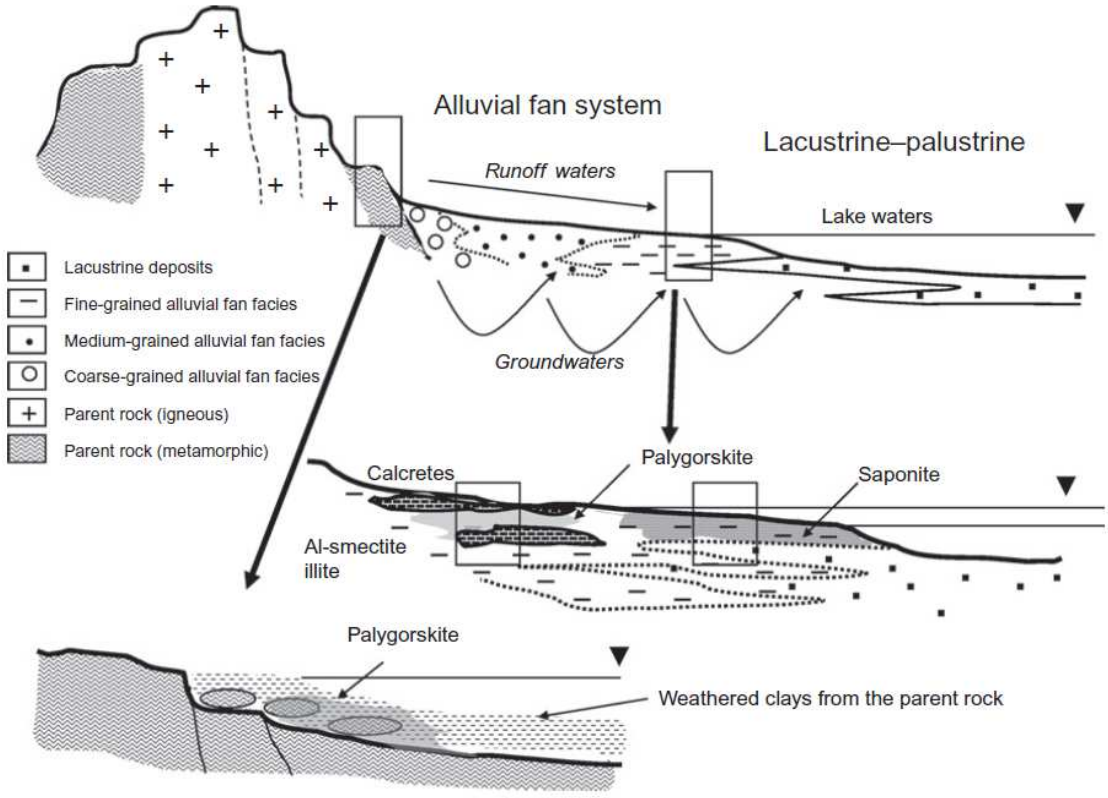

Fig. 17- Environmental model of the genesis of palygorskite.

5.3. Genesis of palygorskite in Formation of Vale do Guizo

The mineralogical and chemical data suggest that palygorskite has been formed by transformation of smectite into palygorskite as it is evident by the inverse relationship between two minerals (further study of samples through transmission electron microscopy is needed to show the step by step the transformation phases). Samples S11, S12, S13, S14, SG11, SG12 and SG14 belong to the

alluvial fan facies. Samples SG8, SG9, SG10 and SG13 which are rich in carbonates can be attributed to distal facies (SG13, having calcite as major carbonate) and lacustrine-palustrine environment (SG8, SG9, SG10,having dolomite as major carbonate).

It is interesting to note that an inverse relationship can be established between smectite and palygorskite content (Fig. 18).

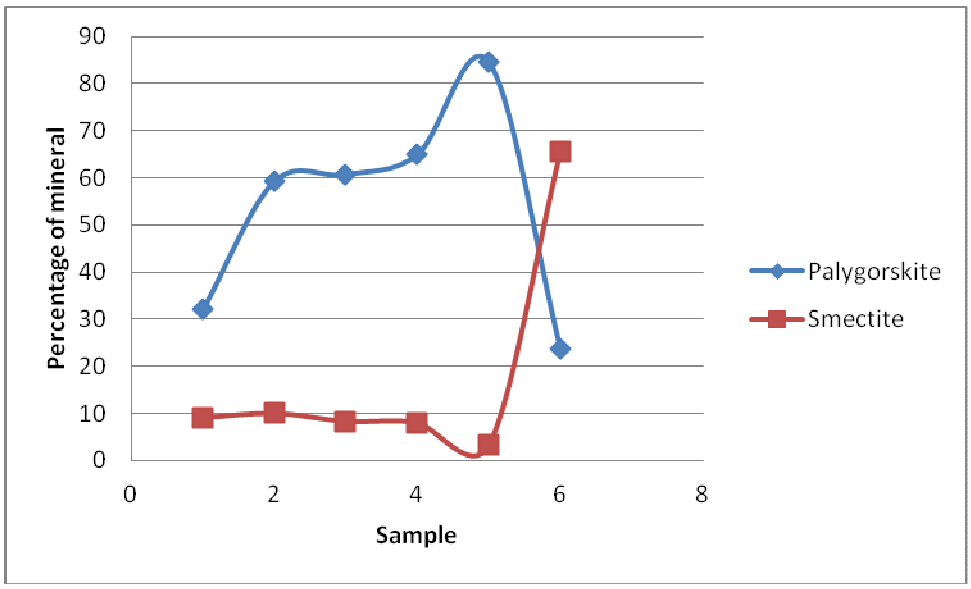

Fig. 18- Relationship between palygorskite and smectite content in the studied samples from Formation of Vale do Guizo, Sado basin.

5.4. Genesis of Palygorskite in Formation of Ervidel

The formation of palygorskite in Formation of Ervidel seems to have been evolved from the transformation of illite into palygorskite as described for palygorskite deposit in Torrejon, Spain (Galan *et al.,* 1975; Galan & Castillo, 1984), by degradation of schist illite and chlorite under acid conditions, and subsequent Mg fixing in the basin in an alkaline environment. Samples S4, SG4, SG5, SG6 and SG7 belong to the alluvial fan facies. Samples S1, S2, S3, SG1 and SG2 which are rich in carbonates can be attributed to distal facies and lacustrine-palustrine environment (SG3) having dolomite as major carbonate.

It is interesting to note here that an inverse relationship can be established between palygorskite and illite amount in this formation instead of palygorskite and smectite content as in Formation of Vale do Guizo (Fig. 19).

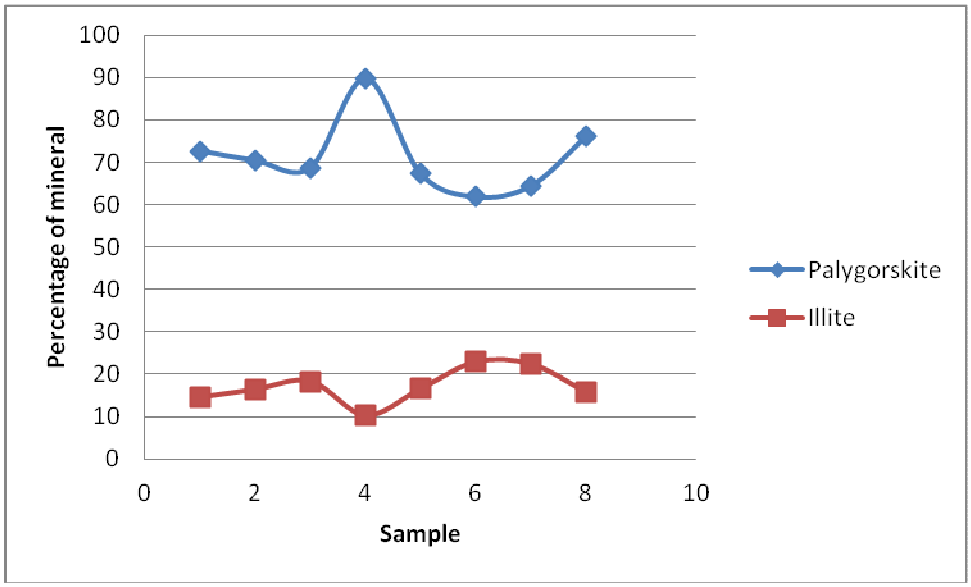

Fig. 19- Relationship between palygorskite and illite content in the studied samples from Formation of Ervidel, Sado basin.

The presence of palygorskite in Formation of Ervidel and Formation of Vale do Guizo is evident of arid to semi arid paleoclimate with the installation of small mudflats in the middle of basin during the time of deposition of these formations during Eocene. The typical fluvial fan system progrades to western part of the basin into palustrine environment.

6. References

Adatte, T., Bolle, M.P. 2001. Palaeocene–early Eocene climatic evolution in the Tethyan realm: clay mineral evidence. Clay Minerals 36, 249–261.

Alcalá, F.J., Martín-Martín, M., López-Galindo, A. 2001. Clay mineralogy of the Tertiary sediments in the Internal Subbetic of Málaga Province, S Spain: implications for geodynamic evolution. Clay Minerals 36, 615–620.

Boillot, G., Montadert, L., Lemoine, M., Bijou-Duval, B. 1984. Les Marges Continentales Actuelles et Fossiles Autour de la France. Masson Ed., Paris, 342 pp.

Brindley, G. and Brown, G. 1980. Crystal Structure of Clay Minerals and their X-ray identification. S.l, Mineralogical Society.

Brisset, F. 2008. Microscopie électronique à balayage et Microanalyses. EDP Sciences.

Callen, R.A. 1984. Clays of the palygorskite–sepiolite group: depositional environment, age and distribution. In: Singer, A., Gala´n, E. (Eds.), Palygorskite–Sepiolite. Occurrences, Genesis and Uses. Developments in Sedimentology, vol. 37. Elsevier, Amsterdam, pp. 1–37.

Chamley, H. (1989) Clay Sedimentology. Springer- Verlag, Berlin, Heidelberg.

Clark, P.U., Dyke, A.S., Shakun, J.D., Carlson, A.E., Clark, J., Wohlfarth, B., Mitrovica, J.X., Hostetler, S.W., McCabe, A.M. 2009. The last glacial maximum. Science 325, 710–714.

Daoudi, L., Deconinck, J.F., Witan, O., Rey, J. 1995. Impact des variations du niveau marin sur les argiles: exemple du Crétacé inférieur du bassin d'Essaouira (Maroc). Compte Rendue de l'Academie des Science Paris 320, 707–711.

De Galdeano, C.S. 1996. Tertiary tectonic framework of the Iberian Peninsula. In: Friend, P.F., Dabrio, C.J. (Eds.), Tertiary Basins of Spain: The Stratigraphicc Record of Crustal Kinematics. Cambridge Univ. Press, Cambridge, pp. 9– 14.

Dou, Y., Yang, S., Liu, Z., Clift, P.D., Yu, H., Berne, S., Shi, X. 2010. Clay mineral evolution in the central Okinawa Trough since 28 ka: implications for sediment provenance and paleoenvironmental change. Palaeogeography, Palaeoclimatology, Palaeoecology 288, 108–117.

Enu, E.I. 1986. Influence of tectonics and palaeoenvironment on Late Cretaceous clay sedimentation in the Upper Benue Trough, Nigeria. Geological Journal 21, 93–99.

Galán, E. and Singer, A. 2011. Developments in Palygorskite-Sepiolite Research. Volume 3, pp. 1-270.

Galán, E., Castillo, A. 1984. Sepiolite–palygorskite in Spanish tertiary basins: genetical patterns in continental environments. In: Singer, A., Gala´n, E. (Eds.), Palygorskite–Sepiolite. Occurrences, Genesis and Uses. Developments in Sedimentology, vol. 37. Elsevier, Amsterdam, pp. 87–124.

Galan, E., Brell, J.M., la Iglesia, A., Robertson, R.H.S. 1975. The Caceres Palygorskite Deposits, Spain. In: 1975 International Clay Conference. Applied Publ., Mexico, pp. 91–94.

Jones, B.F., Weir, A.H. 1983. Clay minerals of Lake Abert, an alkaline lake. Clays and Clay Minerals 31, 161–172.

Köppen, W., 1936: Das geographische system der klimate, in: *Handbuch der Klimatologie, Vol I, Part C,* Köppen and Geiger (Eds.), Gebrüder Borntraeger, Berlin, 44pp.

Martín-Martín, M., Rey, J., Alcalá, F.J., Tosquella, J., Deramond, J., Lara-Corona, E., Duranthon, F., Antoine, P.O. 2001. Tectonic controls on the deposits of a foreland basin: an example from the Eocene Corbières-Minervois basin, France. Basin Research 13, 419–433.

Merriman, R.J. 2005. Clay minerals and sedimentary basin history. Eur. J. Miner. 17, 7–20.

Moon, J.W., Song, Y., Moon, H.S., Lee, G.H. 2000. Clay minerals from tidal sediments at Youngjong Island, Korea, as a potential indicator of sea-level change. Clay Minerals 35, 841–855.

Pimentel, N.L.V. 2002. Pedogenic and early diagenetic processes in Palaeogene alluvial fan and lacustrine deposits from the Sado Basin (S Portugal). Sedimentary Geology 148, 123–138.

Pimentel, N.L.V. 1998b. Tectono-sedimentary evolution of the Sado Basin (Tertiary, southern Portugal). Comun. Inst. Geol. Mineiro 84 (1), A145– A148.

Pimentel, N.L.V. 1997. The Sado Tertiary Basin. Sedimentological and tectono-sedimentary analysis. PhD thesis, University of Lisbon, Lisbon.

Rocha, 2005. Paleoenvironmental analysis of douro estuary based on mineralogical parameters. Thalassas, An International Journal of Marine Sciences 21 (1), 53-58.

Rodas, M., Luque, F.J., Mas, R., Garzon, M.G. 1994. Calcretes, palycretes and silcretes in the Paleogene detrital sediments of the Duero and Tajo Basins, Central Spain. Clay Minerals 29, 273–285.

Ruffell, A.H., Price, G.D., Mutterlose, J., Kessels, K., Baraboshkin, E., Gröcke, D.R. 2002. Palaeoclimate indicators (clay minerals, calcareous nannofossils, stable isotopes) compared from two successions in the late Jurassic of the Volga Basin (SE Russia). Geological Journal 37, 17–33.

Singer, A. 1984. Pedogenic palygorskite in the arid environment. In: Singer, A., Galán, E. (Eds.), Palygorskite–Sepiolite. Occurrences, Genesis and Uses. Developments in Sedimentology, vol. 37. Elsevier, Amsterdam, pp. 169–177.

Tapponier, P. 1977. Evolution tectonique du syste`me alpin en Mediterrane ´e: poinconnement et e´crasement rigide-plastique. Bull. Soc. Geol. Fr. 7 (19), 437–460.

Thiry, M., Jacquin, T. 1993. Clay mineral distribution related to rift activity, sea-level change and palaeoceanography in the Cretaceous of the Atlantic Ocean. Clay Minerals 28, 61–84.

Uchupi, E. 1988. The Mesozoic– Cenozoic evolution of Iberia. A tectonic link between Africa and Europe. Rev. Soc. Geol. Esp. 1 (3/4), 257–294.

Wang, Z., Chen, Z., Tao, J. 2006. Clay mineral analysis of sediments in the Changjiang Delta Plain and its application to the Late Quaternary variations of sea level and sediment provenance. Journal of Coastal Research 22, 683–691.

Weaver, C.E. 1989. Clays, Muds and Shales. Elsevier, The Netherlands.

Annex-Diffractograms of Samples

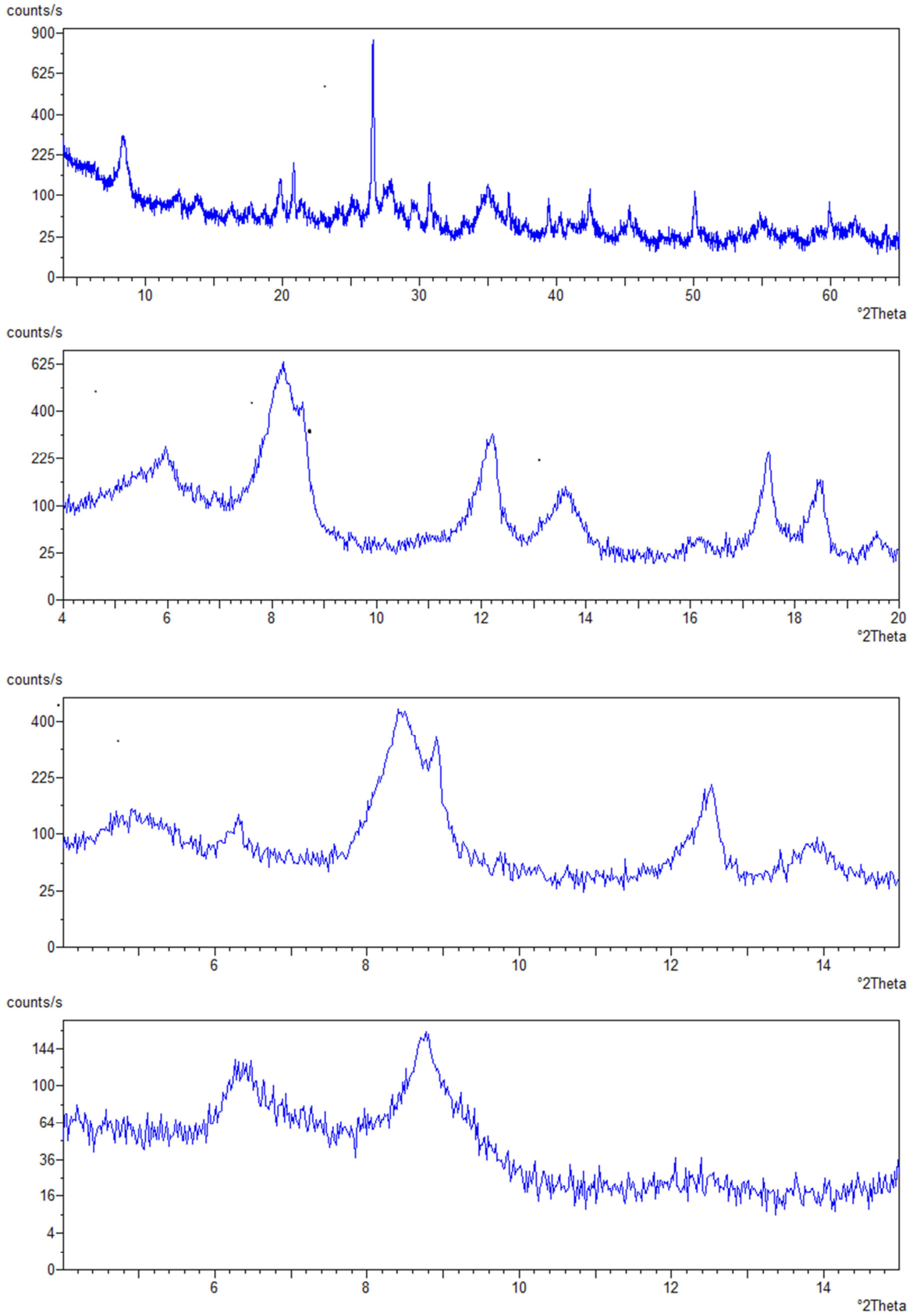

Fig.20- Diffractogarms of sample S1, powder, natural, glycolated and at 500°C.

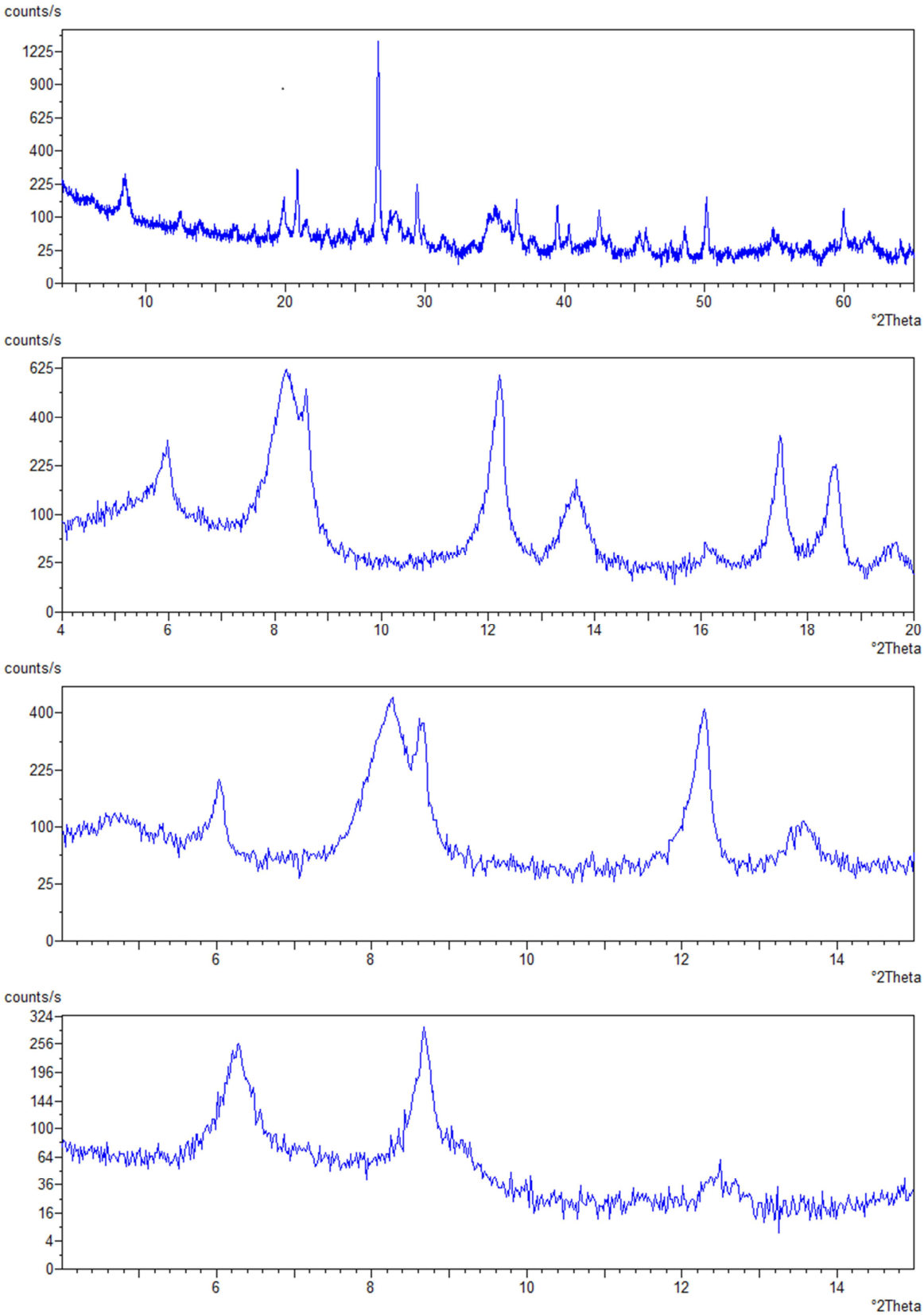

Fig.21- Diffractogarms of sample S2, powder, natural, glycolated and at 500°C.

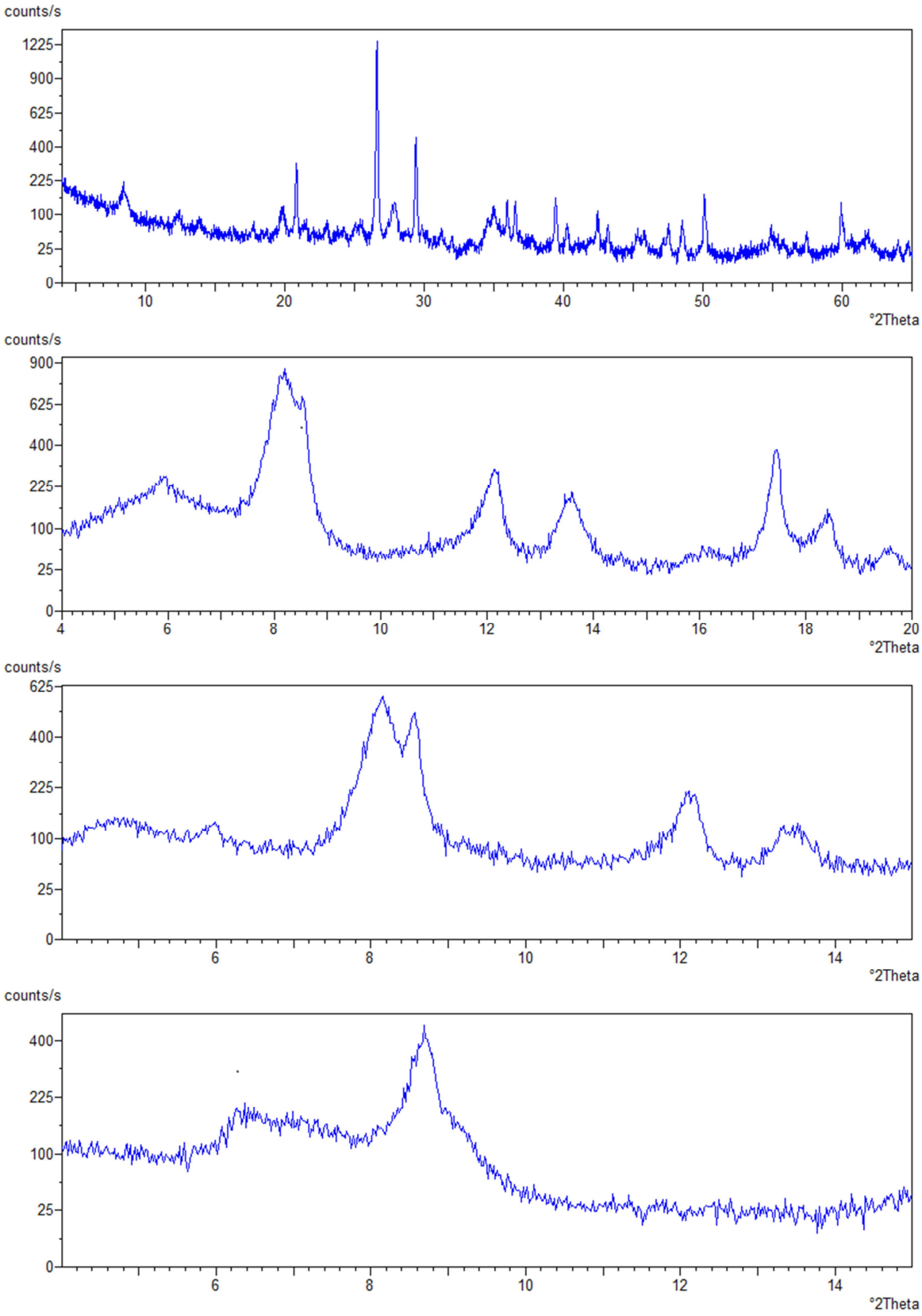

Fig.22- Diffractogarms of sample S3, powder, natural, glycolated and at 500°C.

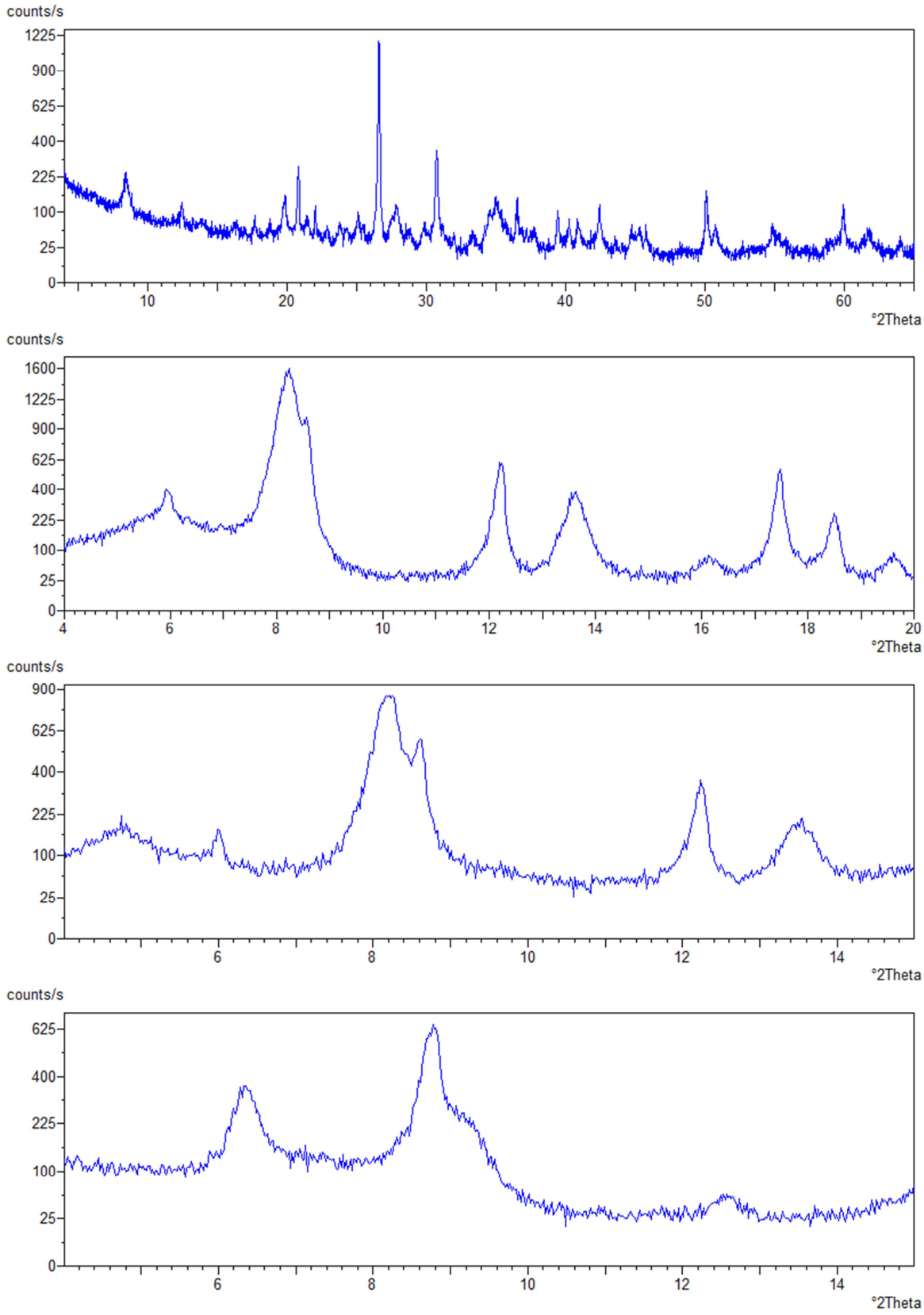

Fig.23- Diffractogarms of sample S4, powder, natural, glycolated and at 500°C.

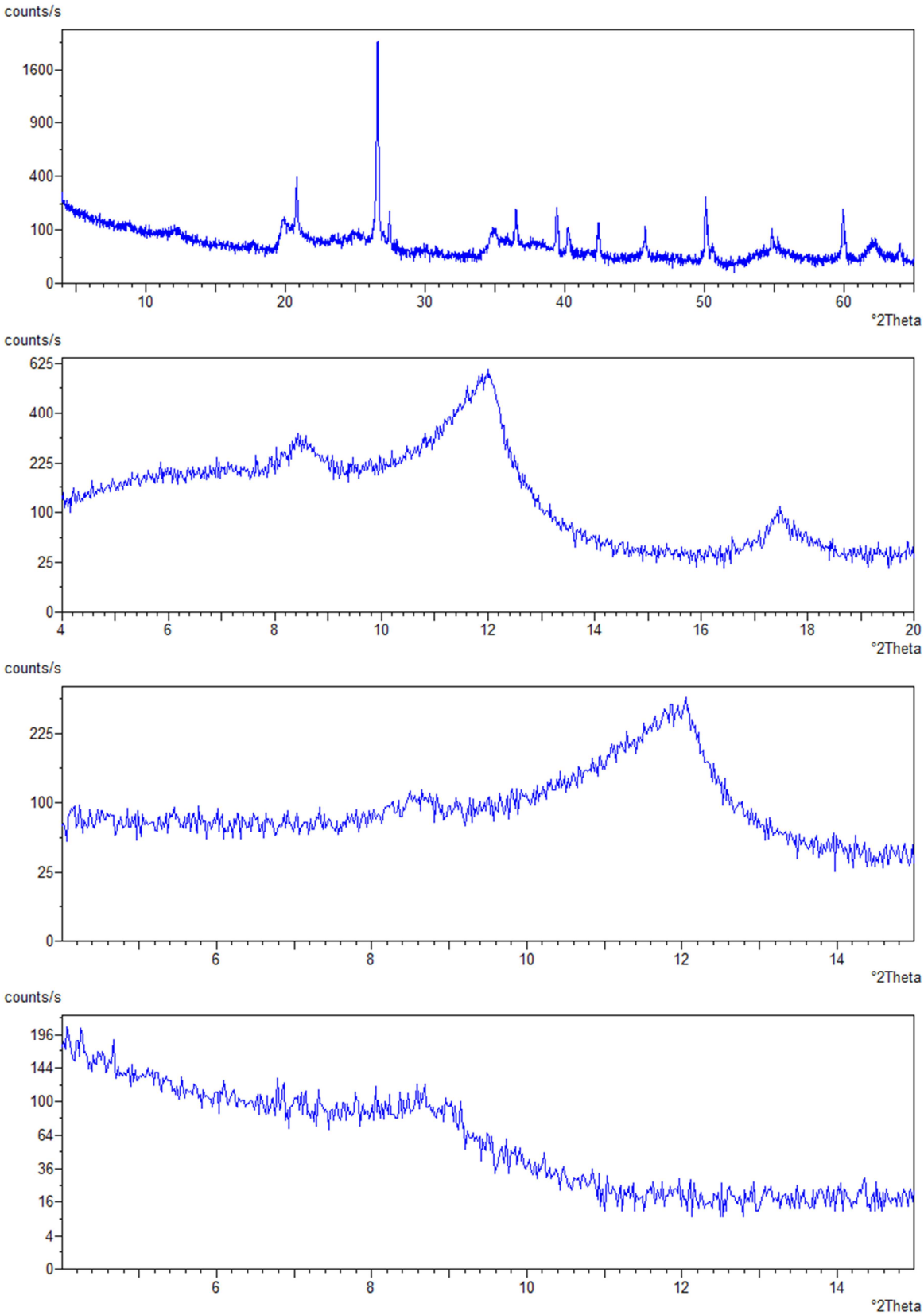

Fig.24- Diffractogarms of sample S5, powder, natural, glycolated and at 500°C.

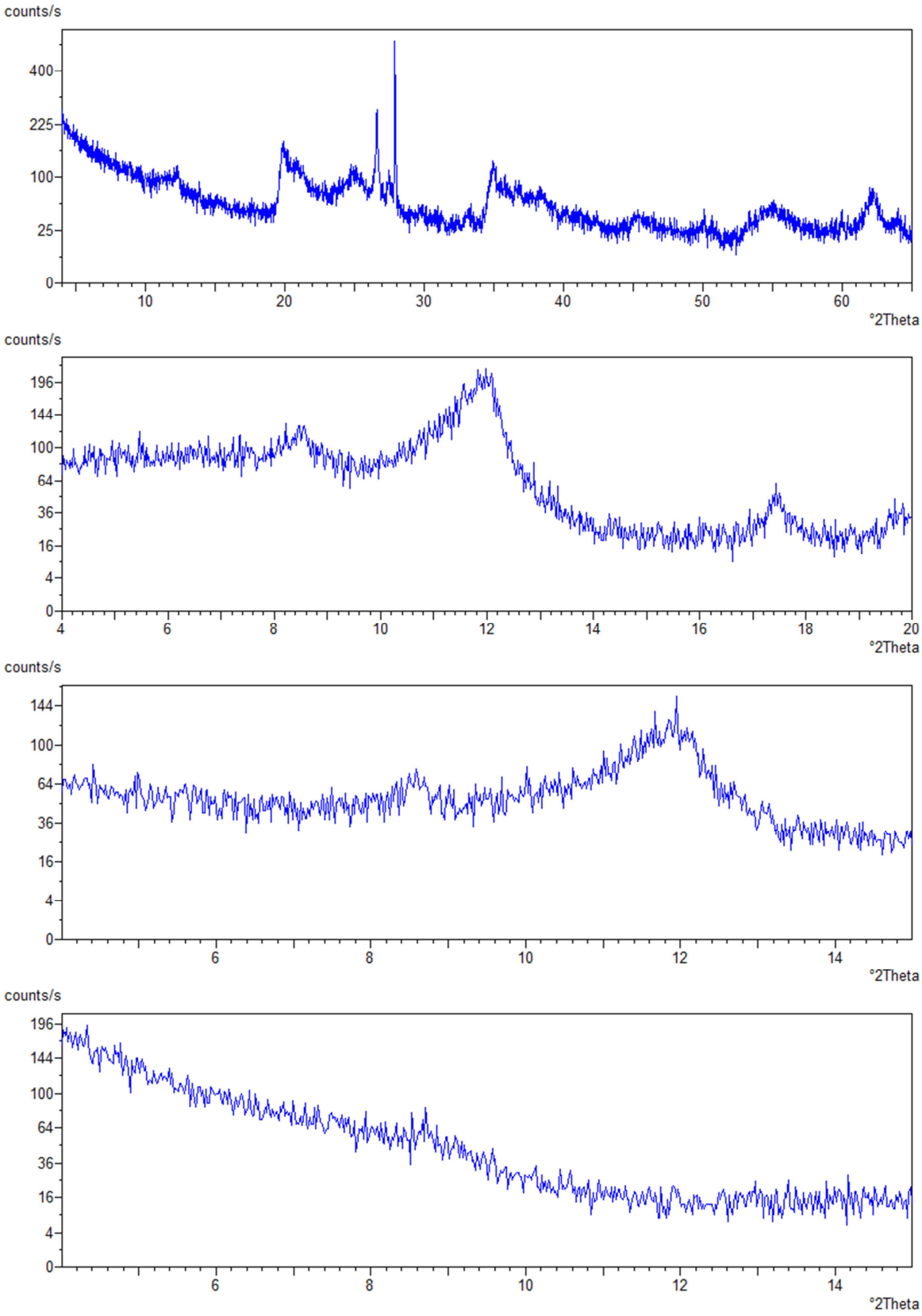

Fig.25- Diffractogarms of sample S6, powder, natural, glycolated and at 500°C.

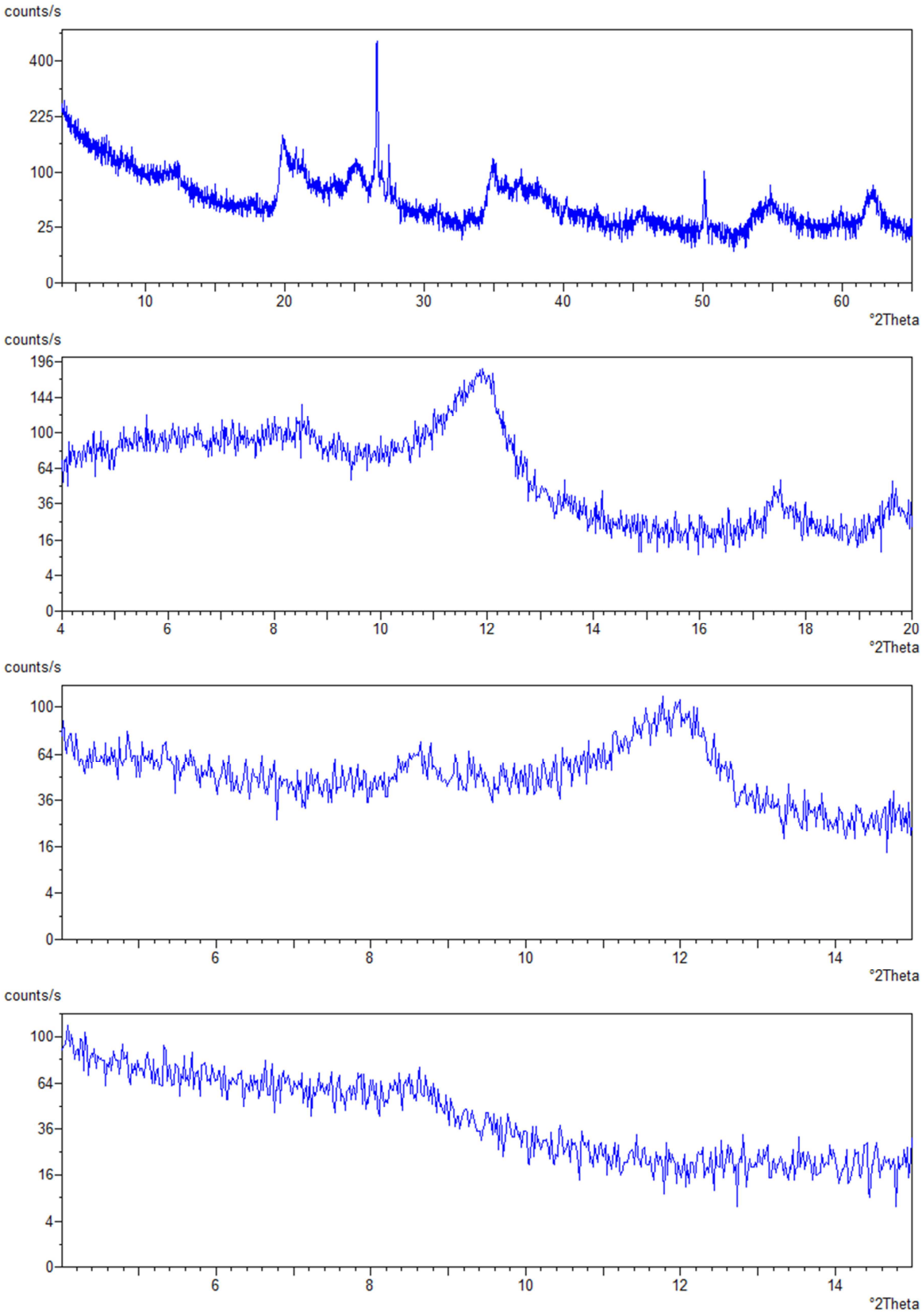

Fig.26- Diffractogarms of sample S7, powder, natural, glycolated and at 500°C.

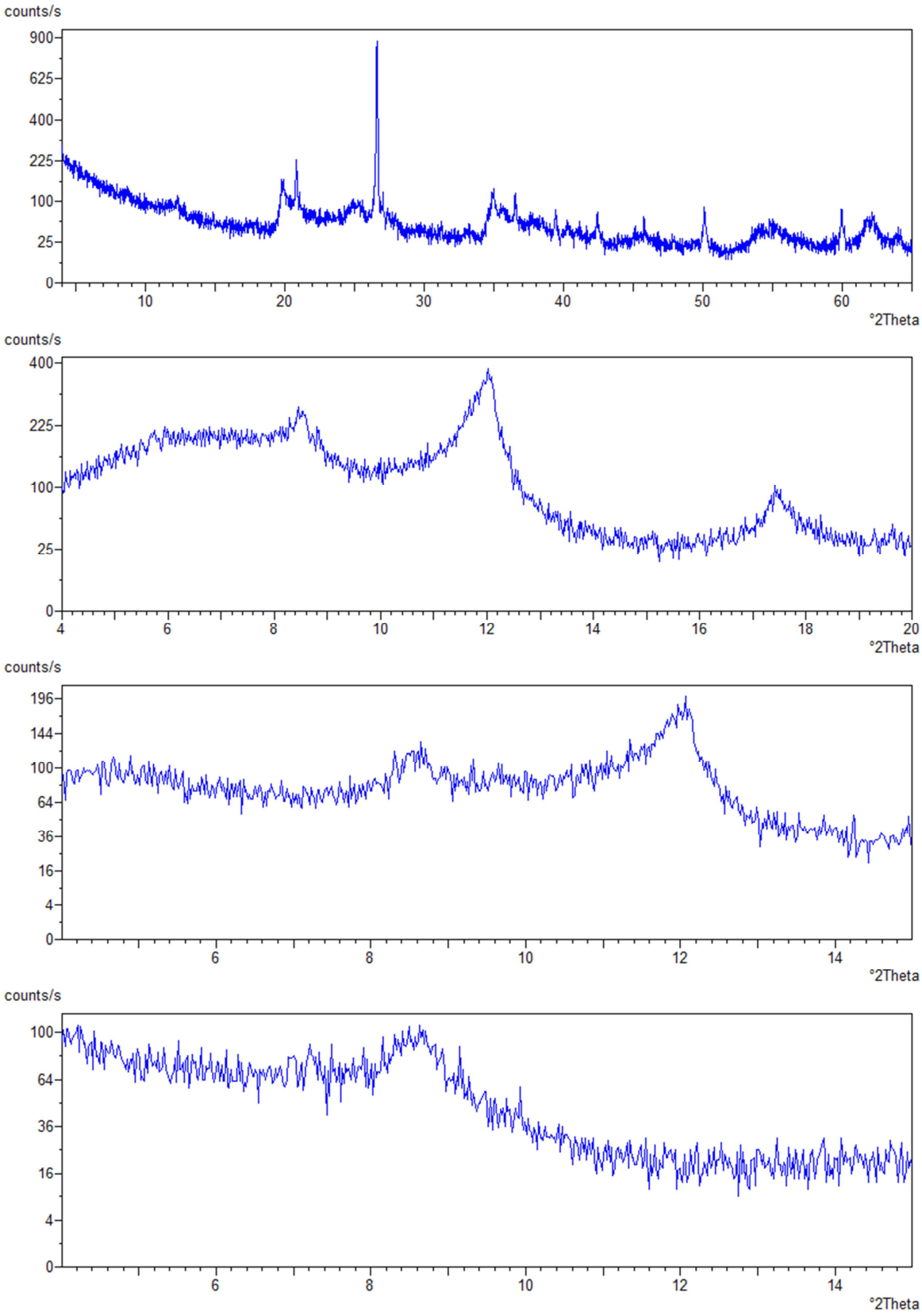

Fig.27- Diffractogarms of sample S8, powder, natural, glycolated and at 500°C.

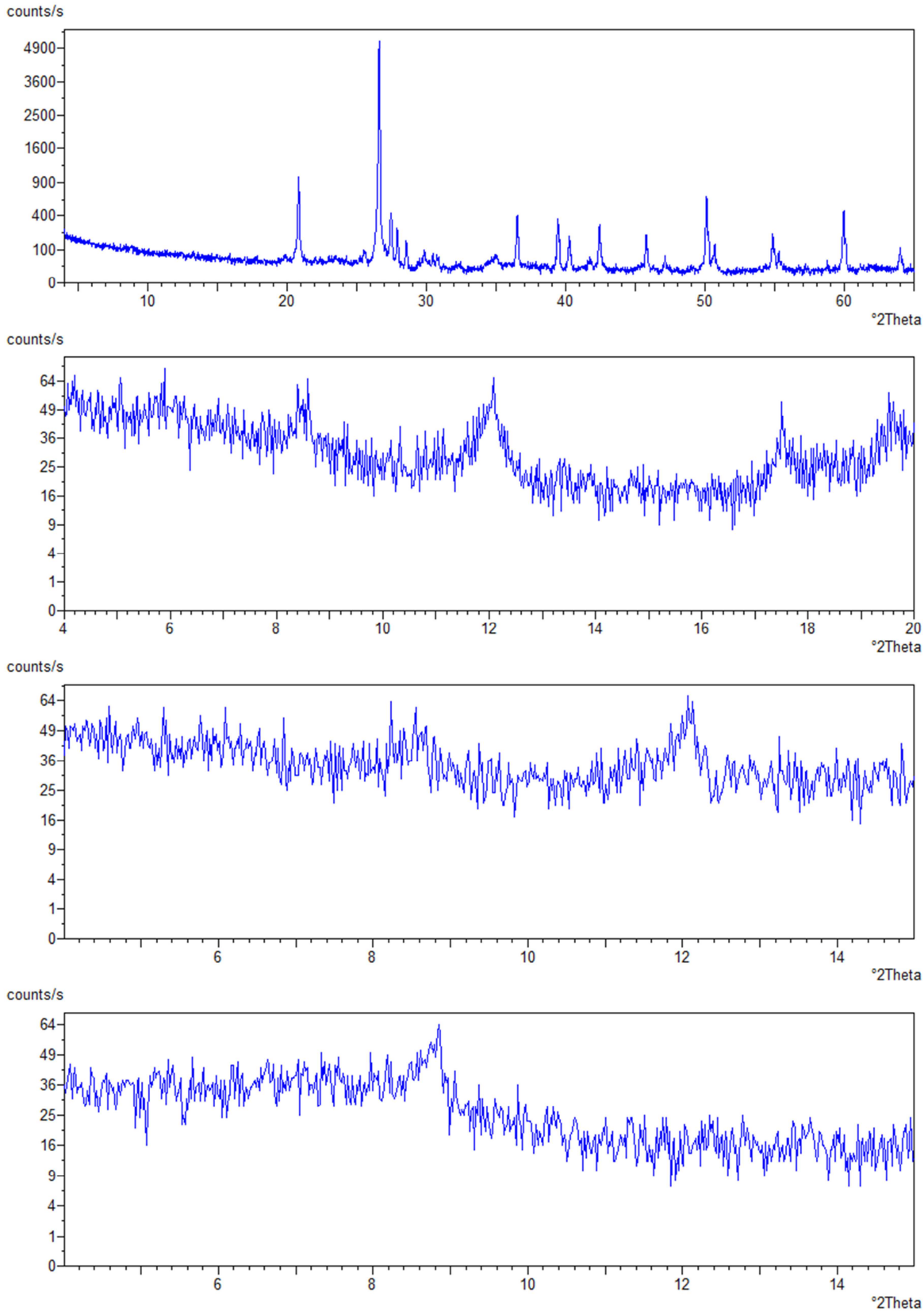

Fig.28- Diffractogarms of sample S9, powder, natural, glycolated and at 500°C.

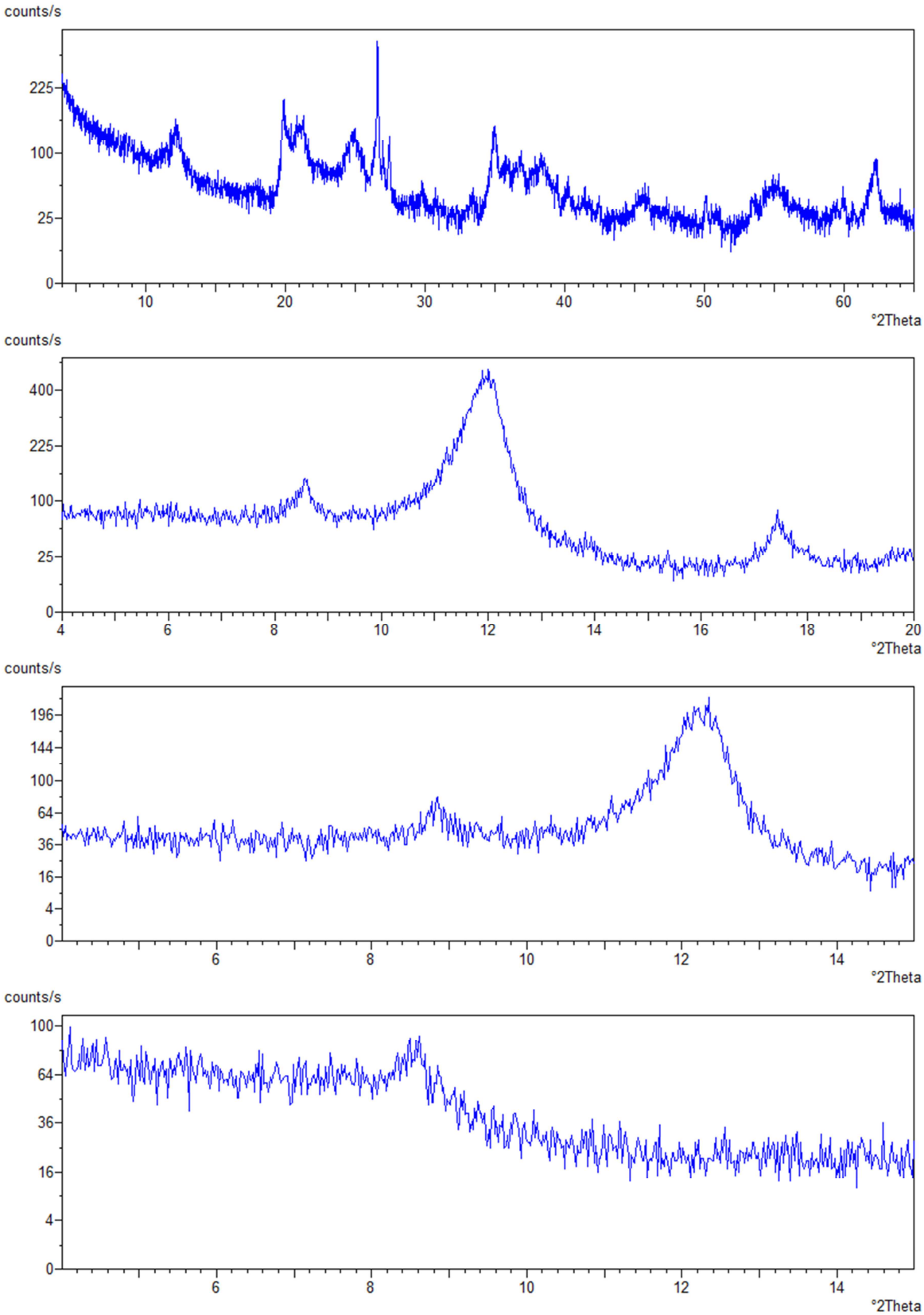

Fig.29- Diffractogarms of sample S10, powder, natural, glycolated and at 500°C.

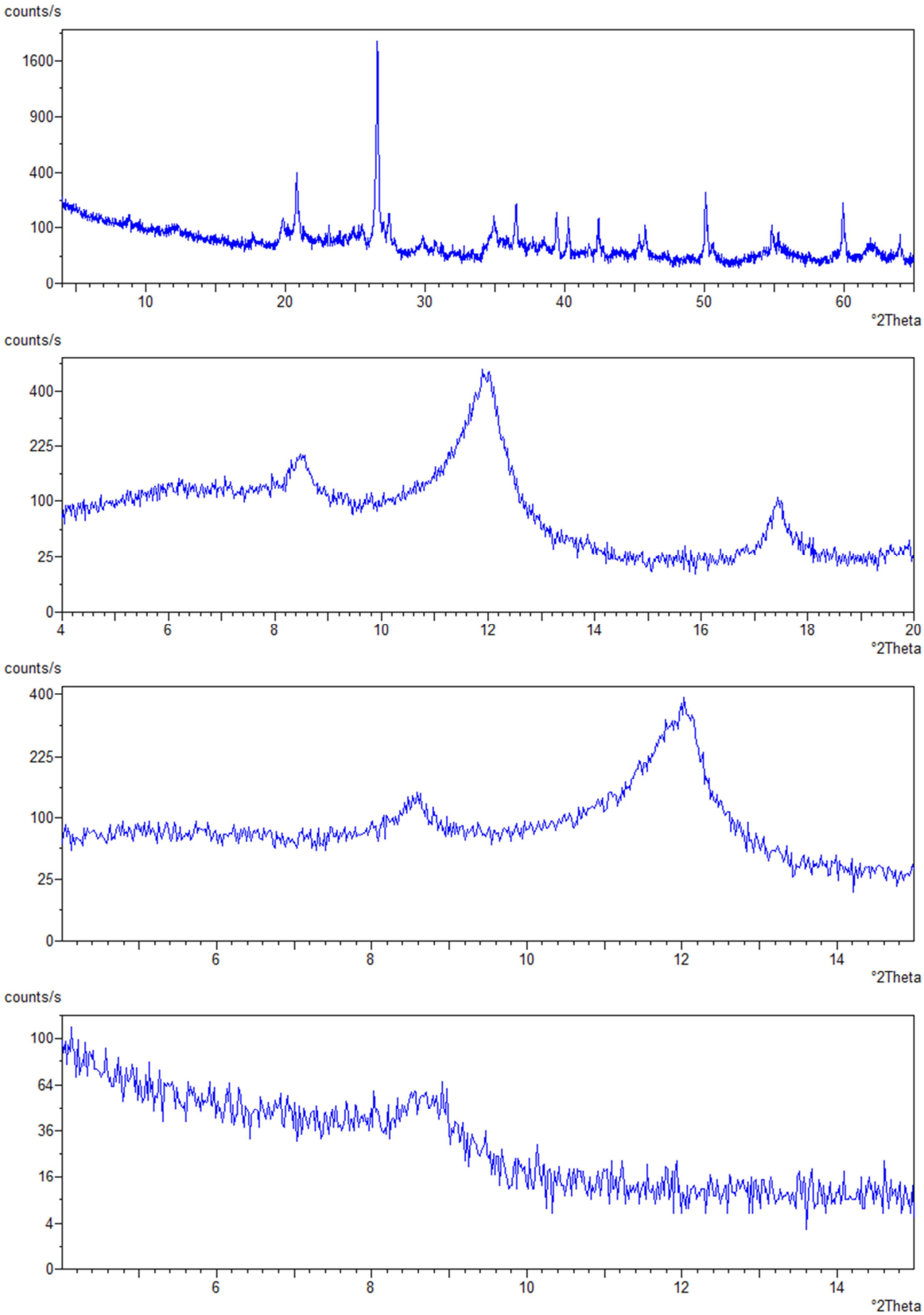

Fig.30- Diffractogarms of sample S11, powder, natural, glycolated and at 500°C.

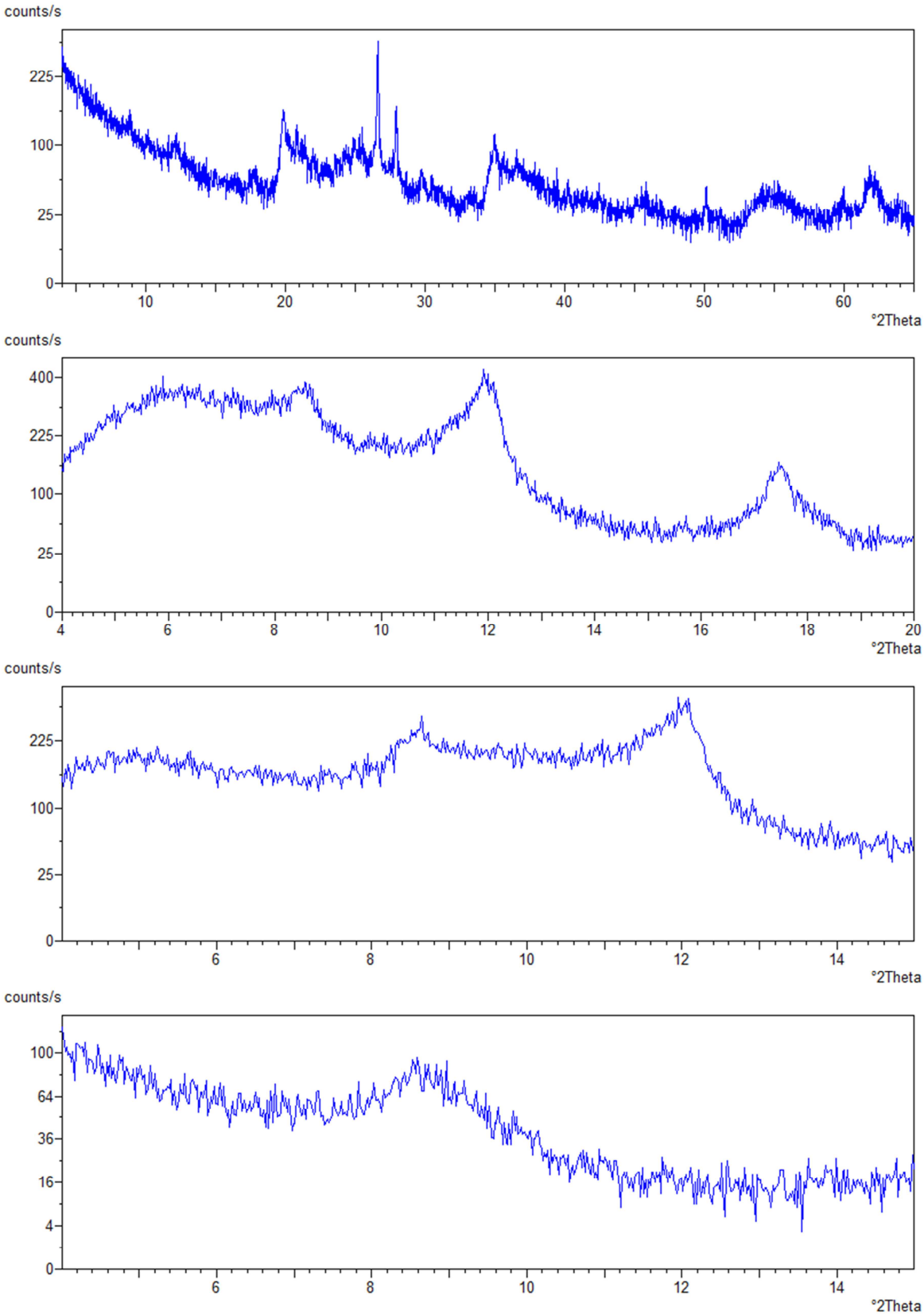

Fig.31- Diffractogarms of sample S12, powder, natural, glycolated and at 500°C.

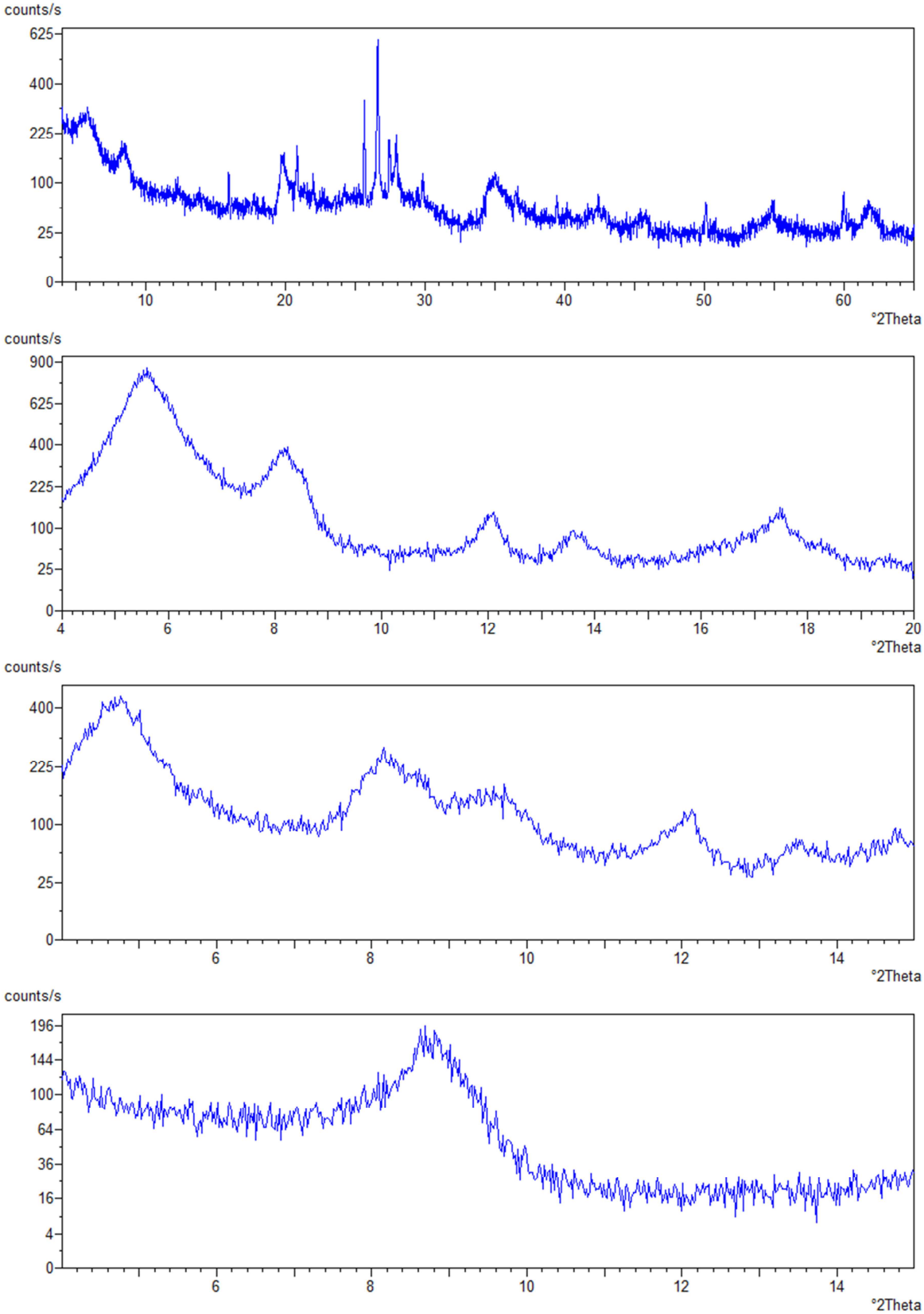

Fig.32- Diffractogarms of sample S13, powder, natural, glycolated and at 500°C.

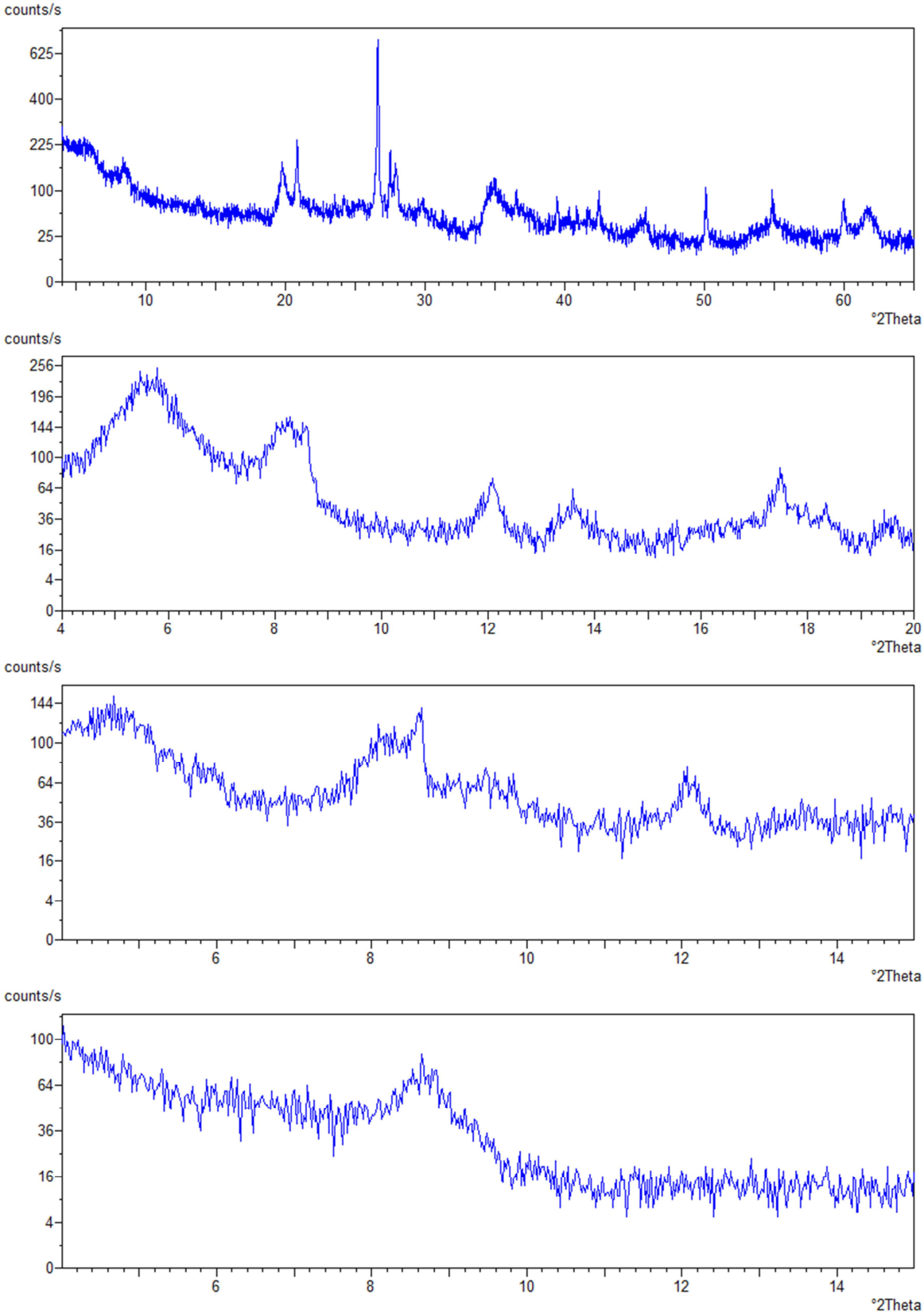

Fig.33- Diffractogarms of sample S14, powder, natural, glycolated and at 500°C.